Transcription initiation mapping in 31 bovine tissues reveals complex promoter activity, pervasive transcription, and tissue-specific promoter usage

Goszczynski D.E.[1,2], Halstead M.M.[1,2], Islas-Trejo A.D.[1], Zhou H.[1], Ross P.J.[1]

[1] Department of Animal Science, University of California, Davis, CA, USA 95616

[2] Both authors contributed equally to this work

Corresponding author: Ross PJ, pross@ucdavis.edu

Running title: TSS mapping in the bovine genome

Keywords: transcription start sites, RAMPAGE, cattle, promoter, atlas

ABSTRACT

Characterizing transcription start sites is essential for understanding the regulatory mechanisms that control gene expression. Recently, a new bovine genome assembly (ARS-UCD1.2) with high continuity, accuracy, and completeness was released; however, the functional annotation of the bovine genome lacks precise transcription start sites and includes a low number of transcripts in comparison to human and mouse. Using the RAMPAGE approach, this study identified transcription start sites at high resolution in a large collection of bovine tissues. We found several known and novel transcription start sites attributed to promoters of protein coding and lncRNA genes that were validated through experimental and *in silico* evidence. With these findings, the annotation of transcription start sites in cattle reached a level comparable to the mouse and human genome annotations. In addition, we identified and characterized

transcription start sites for antisense transcripts derived from bidirectional promoters, potential lncRNAs, mRNAs, and pre-miRNAs. We also analyzed the quantitative aspects of RAMPAGE data for producing a promoter activity atlas, reaching highly reproducible results comparable to traditional RNA-Seq. Lastly, gene co-expression networks revealed an impressive use of tissue-specific promoters, especially between brain and testicle, which expressed several genes in common from alternate transcription start sites. Regions surrounding co-expressed modules were enriched in binding factor motifs representative of their tissues. This annotation will be highly useful for future studies on expression control in cattle and other species. Furthermore, these data provide significant insight into transcriptional activity for a comprehensive set of tissues.

INTRODUCTION

With the advent of new sequencing technologies, genomics has emerged as one of the most promising fields in biology. Since its implementation in breeding schemes, livestock industries have seen enormous improvements in productivity (Van Eenennaam et al. 2014), and genomics are expected to play a key role in improving animal welfare, protecting the environment, and securing high quality food for a growing human population (Britt et al. 2018). For genomic approaches to succeed, the quality of reference genomes is essential. The first bovine genome was published in 2009 (Consortium et al. 2009). Its publication and the improvements that followed have allowed the application of genomic technologies aimed at genetic improvement (Null et al. 2019), the study of molecular and physiological mechanisms of animal health and disease (Ju et al. 2020), and the development of genome engineering approaches (Bevacqua et al. 2016). Recently, a new version of the bovine genome, ARS-UCD1.2, was assembled using single molecule sequencing, increasing the continuity, accuracy, and completeness compared to its predecessor (Rosen et al. 2020). With a more reliable genome reference, the focus now

transitions from genome sequence to genome annotation, where a comprehensive identification of the expressed components of the genome is utterly necessary. The annotation of functional regulatory elements in cattle, as well as other important agricultural species, is one of the main objectives of the international Functional Annotation of Animal Genomes (FAANG) Consortium (www.faang.org) (Andersson et al. 2015).

A key step to study transcription regulation is the elucidation of transcription start sites (TSSs), as these loci harbor transcription factor binding sites that dictate gene expression and integrate the inputs from other cis-regulatory elements (e.g., enhancers). Generally, TSSs are amidst an epigenetic landscape that involves chromatin accessibility (Meers et al. 2018), and H3K4me3 and H3K27ac histone marks (Ernst and Kellis 2017). These epigenetic characteristics can be used to differentiate promoters from other gene regulatory regions, such as enhancers, which are typically enriched in additional histone marks such as H3K4me1 (Ernst and Kellis 2017). Methods to study 5' ends of transcripts, and thus the initiation of transcription, have been based on the capture of 5' caps or the preferential ligation of adapters to it (Batut et al. 2013; Kodzius et al. 2006; Salimullah et al. 2011; Yamashita et al. 2011). This distinction is important as mRNA is reverse transcribed (RT) from 3' end to 5' end, and the 5' end can be underrepresented in conventional RNA-Seq data, especially if oligo-dT primers were used in the RT reaction. The RAMPAGE technique (RNA Annotation and Mapping of Promoters for the Analysis of Gene Expression) is an accurate 5'-complete cDNA sequencing approach that allows for the *ab initio* identification of transcription start clusters (TSCs) at single base pair resolution and the quantification of their expression (Batut et al. 2013). One of the main advantages of this technique is that it makes use of paired end information, allowing the attribution of TSCs to genes based on sequences at both sides of the fragment, and the discrimination of nonspecific signal caused by incomplete cDNAs through the modeling of transcript abundance by downstream coverage (Batut et al. 2013).

Considering the start coordinate of an annotated transcript as the transcription start site (TSS), the ARS-UCD1.2 bovine genome annotation from the Ensembl database (release 95) includes 39,705 TSSs for protein coding or lncRNA transcripts: a low number in comparison to the 139,158 TSSs annotated in human (GRCh38) and the 81,573 TSSs annotated in mouse (GRCm38). Even though small systematic differences are expected in the number of promoters between species, experimental evidence indicates that several bovine transcripts remain to be characterized and annotated (Tong et al. 2017; Weikard et al. 2013). Moreover, studies in mouse and human have demonstrated that a significant proportion of TSSs are enriched in evolutionarily conserved regions (FANTOM Consortium et al. 2014; Abugessaisa et al. 2019), suggesting the number of TSSs in the bovine genome should be higher.

As part of the FAANG consortium, our main objective was to contribute to the bovine transcriptome annotation by identifying TSCs in a large collection of tissues using the RAMPAGE approach. Identified TSCs were validated through several strategies that included experimental evidence from chromatin accessibility assays (ATAC-Seq) and histone modification profiling (ChIP-Seq), which included H3K4me1, H3K4me3, H3K27ac, and H3K27me3. In addition, we evaluated the sequence enrichment for typical promoter elements such as TATA, GC, and CCAAT boxes in regions surrounding TSCs, and known tissue-specific transcription factor binding motifs. Based on signal in TSCs, RAMPAGE data were also used to produce a promoter activity atlas, and comparison of RAMPAGE with traditional RNA-seq revealed highly consistent and reproducible expression quantification. Unassigned TSCs with insufficient evidence to be attributed to a gene were screened through a set of bioinformatic tools to predict their potential role in the genome, including whether they corresponded to unannotated mRNAs, pre-miRNAs, and ncRNAs. These elements were particularly interesting due to their antisense activity. Lastly, expression data derived from the RAMPAGE signal was

used to generate co-expression networks and to characterize the use of alternative TSCs across tissues.

RESULTS

Dataset complexity

A total of 111 biological samples corresponding to 31 different tissues from two male (M1, M2) and two female (F1, F2) individuals were sequenced in nine batches, resulting in 2.67 billion fragments. In general, a high percentage of fragments from each library (>85%) mapped uniquely to the reference genome, yielding a total of 2.35 billion uniquely mapped fragments (Supplementary Table S1). After duplicate removal, the number of fragments was reduced to 673 million unique sequences, with an average of 6.1 (SD 3.8) million fragments per sample (Figure S1A). A preliminary evaluation by hierarchical clustering based on gene expression (independent of peak calling) identified seven outliers that were discarded from subsequent analyses: abomasum-M1, bladder-F2, colon-F1, esophagus-M1, esophagus-M2, lung-M1, and trachea-M1 (Figure S1B).

---Table S1 submitted as external file due to its size---

Table S1. RAMPAGE alignment summary. Number of input fragments, alignment rates and final number of useful alignments for every sample.

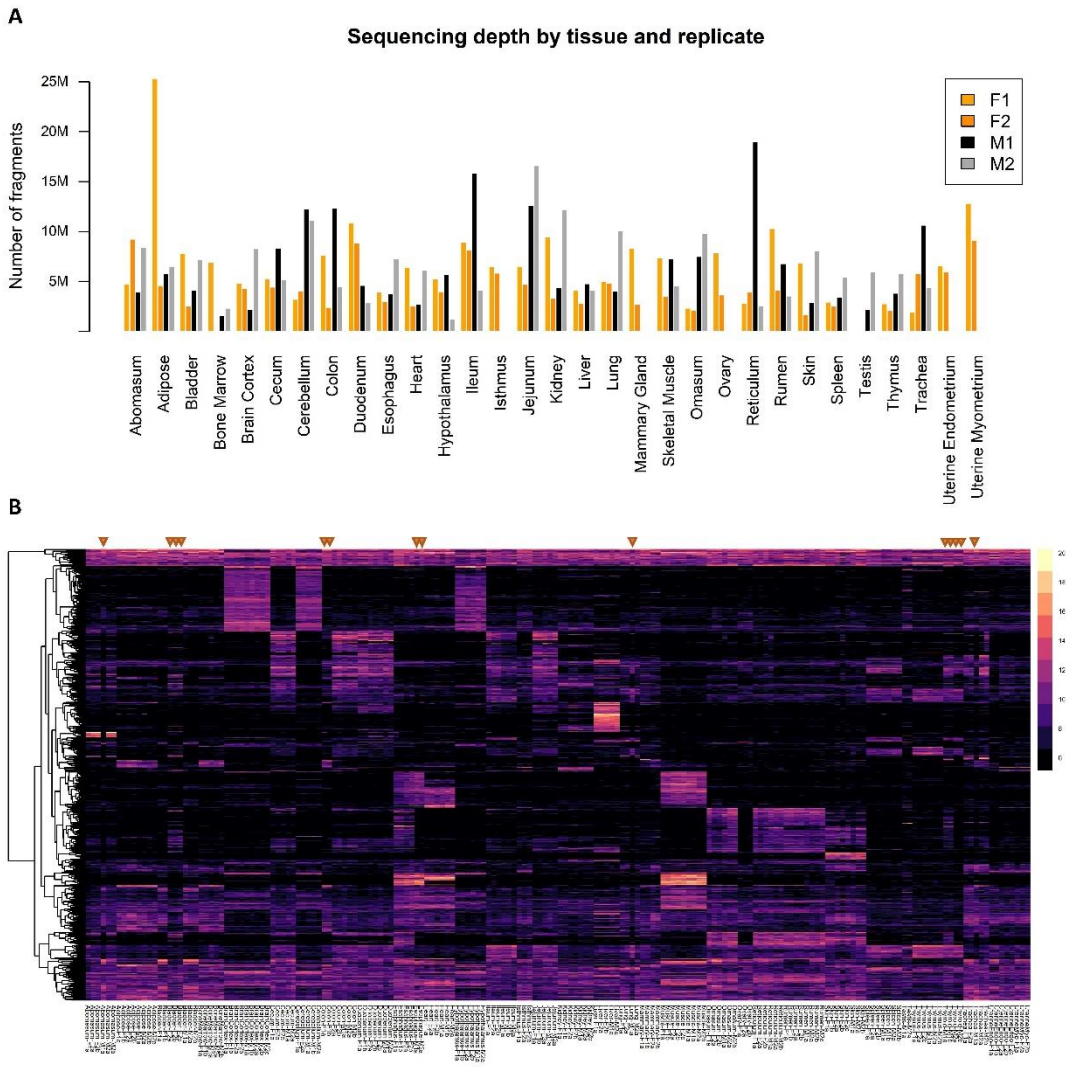

Figure S1. Composition of the dataset used for identification of TSCs in 31 cattle tissues by RAMPAGE sequencing. (A) Sequencing depth by tissue and replicate. The y axis indicates the number of uniquely mapped fragments after duplicate removal. (B) Profiling by gene expression (variance-stabilized counts) showing the unclear identity of the abomasum-M1, bladder-F2, colon-F1, esophagus-M1, esophagus-M2, lung-M1, and trachea-M1 samples (indicated by orange triangles), which were excluded from further analyses.

Identification of TSCs by RAMPAGE

The analysis of 104 samples from 31 tissues from four individuals (two males, two females) identified 93,767 transcription start clusters (TSCs) between the combined dataset (87,553) and single tissue datasets (6,214). TSC size varied from a single base to intervals as broad as 1,089 bp, with most elements falling in the range of 5 to 25 bp (Figure 1A). TSCs identified in the combined dataset were supported by a minimum of 22 independent RAMPAGE tags (Figure 1B), as opposed to tissue-specific TSCs, which were supported by a minimum of three RAMPAGE tags but were conserved between biological replicates.

The bovine genome annotation (Ensembl release 95) considered for this study comprised 33,019 and 31,052 different TSSs and transcription termination sites (TTSs), respectively, associated with 23,328 protein coding or long noncoding (lncRNA) genes. To account for nonspecific transcription initiation, TSSs were defined as start coordinate ± 50 bp. The annotation contained 99 TSSs overlapping with TTSs, 1,676 TSSs overlapping with intron-exon boundaries, and 850 TSSs overlapping with exon-intron boundaries. It is worth mentioning that 662 of these TSSs overlapped with boundaries at the end of the first exon due to short exon length.

Most of the TSCs identified in this study were not reported in the Ensembl annotation. In fact, only 12,072 (13%) of the TSCs overlapped with previously annotated TSSs (Figure 1C). In order to determine whether the remaining 19,781 annotated TSSs were undetected or shifted with respect to the annotation, we analyzed their gene expression and, in case of presenting expression values higher than 3 counts per million (CPM), we mapped their location relative to RAMPAGE TSCs. No expression was detected for 3,620 (16%) of the annotated genes, which corresponded to 3,718 annotated TSSs. The location of the remaining 16,063 nonoverlapped TSSs around TSCs suggested that 44% of these elements were shifted by a margin of 200 bp (Figure S2). No TSC enrichment was observed in the vicinity of TTSs (Figure 1D). On the other

hand, several TSCs were found to overlap with internal annotated intron-exon (2,148) (Figure 1E) and exon-intron boundaries (299) at least by one base (Figure 1F).

To exclude the possibility that boundary associated TSCs surged as a consequence of transcript fragmentation or capture of partial splicing products, we investigated the chromatin accessibility and histone mark profile of the same tissue in which the TSC was active. This analysis revealed the presence of transcriptional activation marks (H3K4me3, H3K27ac) and accessible chromatin (ATAC-seq) at the discovered TSC sites, while internal intron-exon and exon-intron boundaries showed no enrichment for these marks (Figure S3, Supplementary Material).

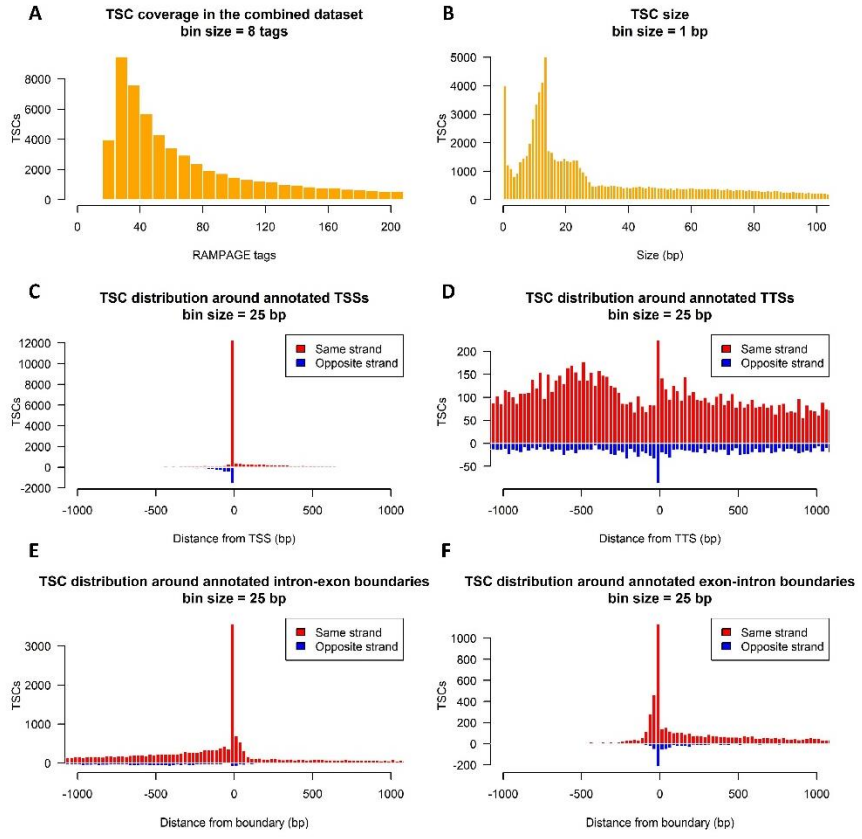

Figure 1. Identification of promoters by RAMPAGE. (A) Tag coverage in TSCs identified in the combined dataset. (B) TSC size distribution for the whole dataset. (C) Histogram of the distance

between TSC and the nearest annotated TSS. (D) Histogram of the distance between TSC and the nearest annotated TTS. (E) Histogram of the distance between TSCs located close to an intron-exon boundary and the corresponding boundary. Only intron-exon boundaries not overlapping with any annotated TSSs were considered. (F) Histogram of the distance between TSCs located close to an exon-intron boundary and the corresponding boundary. For visualization, exon-intron boundaries corresponding to the first exon were ignored, as TSCs tended to group immediately upstream of these boundaries and interfere with the visualization.

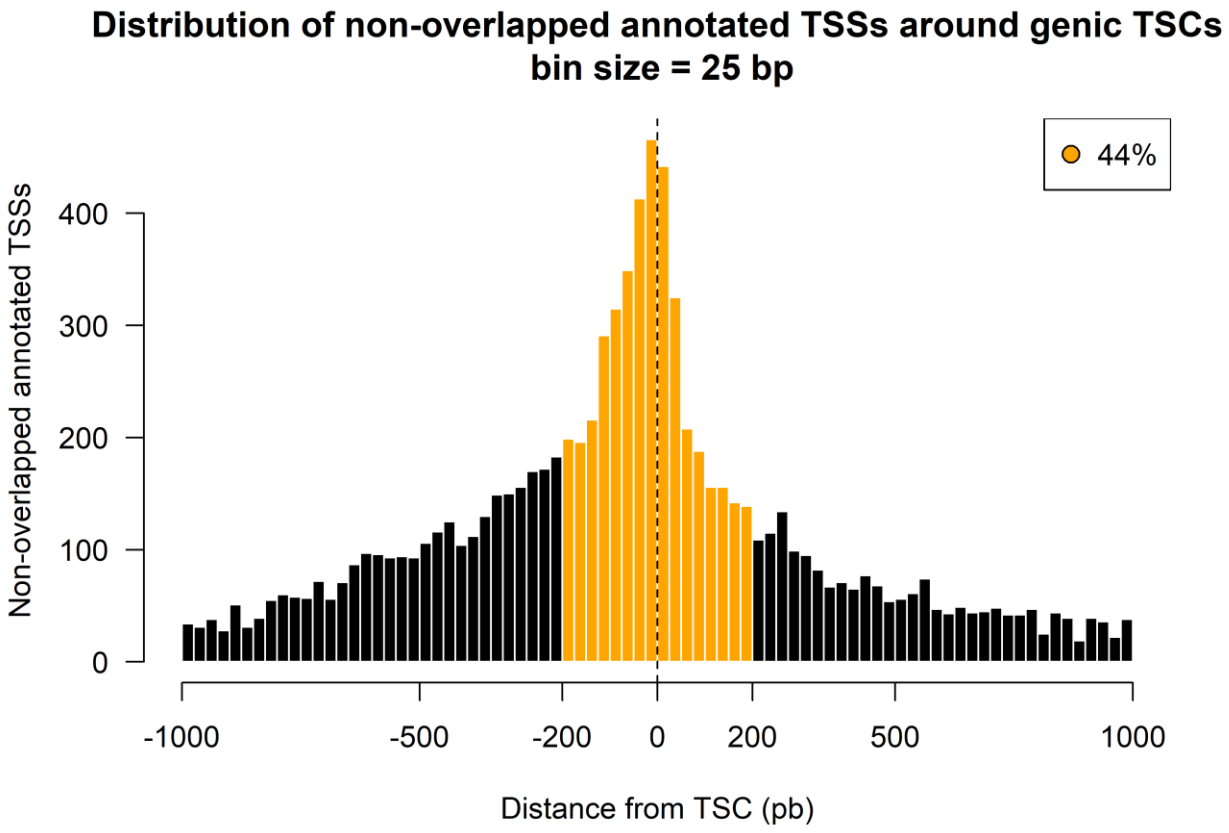

Figure S2. Distribution of nonoverlapped TSSs relative to genic TSCs identified by RAMPAGE. Many of the annotated TSS were shifted with respect to TSCs (orange), while the rest (black) likely belonged to transcripts variants undetected in our dataset. Only annotated genes with high expression levels (CPM > 3) were considered for this figure.

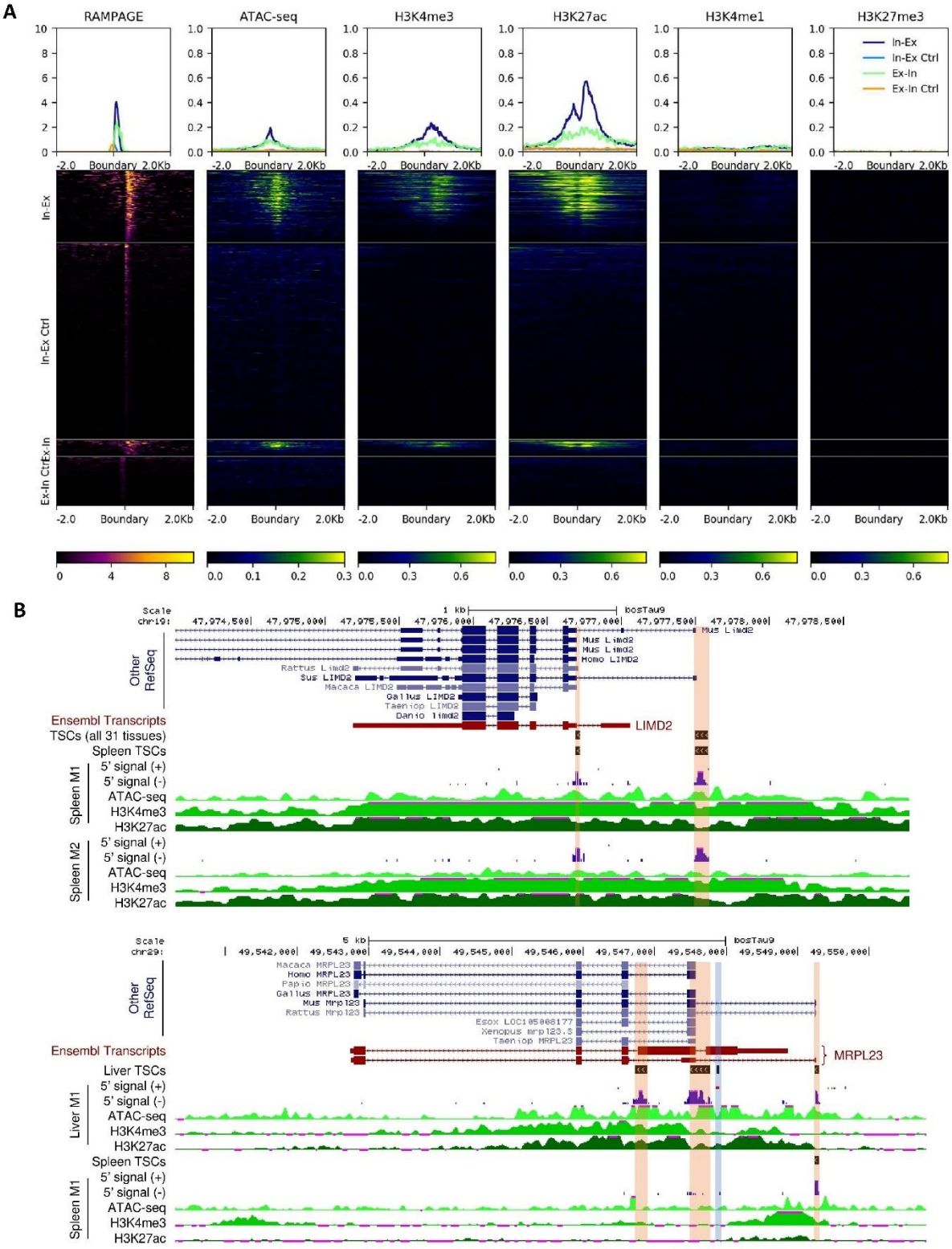
A
RAMPAGE
ATAC-seq
H3K4me3
H3K27ac
H3K4me1
H3K27me3
In-Ex
In-Ex Ctrl
Ex-In
Ex-In Ctrl
Boundary 2.0Kb
B
Other RefSeq
Ensembl Transcripts
LIMD2
TSCs (all 31 tissues)
Spleen TSCs
Spleen M1
Spleen M2
5' signal (+)
5' signal (-)
ATAC-seq
H3K4me3
H3K27ac
MRPL23
Liver TSCs
Liver M1

`

Figure S3. Chromatin accessibility and histone marks at intron-exon and exon-intron boundaries associated with TSCs (Lung-M2). (A) Distribution of reads from different assays over a window of 2 kb to each side of the boundaries. The RAMPAGE signal contemplates only the first read of the pair (R1). Panels 'In-Ex' and 'Ex-In' represent intron-exon and exon-intron boundaries overlapped by TSCs and expressed at a minimum level of 3 CPM with respect to all RAMPAGE tags. Control regions (Ctrl) comprised boundaries from the same transcripts, covered by at least 3 fragments, and located at least 2 kb away from the nearest TSC to avoid signals from near TSCs. Heatmaps are colored according to CPM values. Profiles above heatmaps represent the median signal at each coordinate of the 4kb window. The co-occurrence of chromatin accessibility (ATAC-Seq) and transcriptional activation marks (H3K4me3, H3K27ac), and the absence of enhancer (H3K4me1) and repressive (H3K27me3) marks at the TSC sites implicated these boundaries as putative promoters. The remaining tissue samples are available as supplementary material. (B) 5' tags and epigenetic signals at boundary-associated TSCs. We found no evidence supporting the annotated TSS for the bovine *LIMD2* gene. In addition, one of the TSCs overlapped an annotated intron-exon boundary. In case of the *MRPL23* gene, we found a highly active TSC at an exon-intron boundary, a second TSC between an exon-intron and an intron-exon boundary, and a third TSC supporting one of the annotated TSSs.

Assignment of TSCs to genes by sequence evidence

Identified TSCs were assigned to genes based on the alignments of their fragments. We associated 46,708 'genic' TSCs with 18,312 protein coding and lncRNA genes, accounting for 78% of the 23,328 annotated genes. In addition to these highly associated TSCs, we identified 3,789 elements weakly associated with 3,176 genes (< 3 reads), 308 of which were absent from the previous list.

The number of genes detected in each biological sample (CPM of genic TSC > 3) varied from 7,841 (muscle-M1) to 11,281 (trachea–M2), with an average of 10,009 genes per sample. Based on the Ensembl annotation, 36% of the genic TSCs were located <2.5 kb upstream of annotated TSSs, 31% were in exons, 23% were in introns, and 10% were intergenic (>2.5 kb from annotated TSS) (Figure 2A). Similar to the global set of TSCs, the size distribution of genic TSCs showed a narrow peak at 1 bp and a broad peak between 5 and 25 bp (Figure 2B).

The assignment of TSCs to genes revealed that 61% of the detected genes were transcribed from more than one site (Figure 2C). We found an average of 2.6 TSC/gene, which was twice the value calculated from the Ensembl annotation (1.3 TSS/gene). Comparatively, our TSC/gene value was between the GRCm38 mouse annotation (2.3 TSS/gene) and the GRCh38 human annotation (2.9 TSS/gene). It is worth mentioning that since RAMPAGE TSCs were identified by merging peaks within windows of 150 bp, we merged annotated TSSs within 150 bp to make comparisons fair.

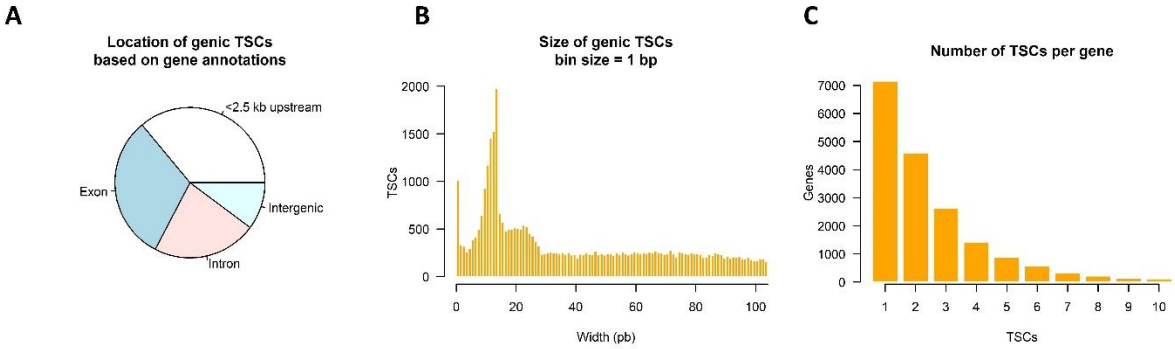

Figure 2. Genic TSCs identified by RAMPAGE sequencing. (A) Location of genic TSCs according to gene annotations. (B) Histogram of TSC size. (C) Use of multiple TSCs for the same gene. Genes with more than ten TSCs were excluded from the plot as they were likely affected by technical artifacts.

Identification of novel promoters

As mentioned previously, most of the genic transcripts in our dataset (34,649) originated from TSCs that were hundreds to thousands of base pairs away from the nearest annotated TSS. To characterize and validate these 'novel' genic TSCs, we studied their location based on gene annotations and their distance to annotated genic TSCs. Then, we evaluated the presence of typical promoter binding motifs and epigenetic marks for transcriptional activation in regions surrounding the TSCs.

According to gene annotations, most of the novel genic TSCs were in exons (38%), followed by introns (30%), regions less than 2.5 kb upstream of annotated TSSs (18%), and intergenic regions (14%) (Figure 3A). Novel genic TSCs were abundant within 1 kb upstream and 2 kb downstream of annotated TSSs (Figure 3B), constituting new alternative sites for transcription initiation in such genes. In terms of expression, novel TSCs contributed substantially to the transcriptome, with half of them driving more than 20% of the total gene expression (Figure 3C).

We then evaluated the characteristics of sequences surrounding novel TSCs (Figure 3D). We found high abundance of TATA-boxes 25 bp upstream of novel TSCs, especially for narrow TSCs (Figure 3E). In general, broad TSCs included more than one TSS, explaining the presence of additional TATA-boxes downstream of the zero coordinate. GC-boxes were highly abundant in broad TSCs and localized mainly at the TSC site and 40 bp upstream. On the other hand, the abundance of CCAAT boxes was relatively low compared to the other marks, but when present, they localized 10-70 bp upstream of broad TSCs. Binding motif enrichment showed these three motifs were significantly enriched in regions 300 bp upstream to 100 bp downstream of novel TSCs compared to other sequences from the genome (p-value ^{TATA} = 1E-61, p-value ^{CCAAT} = 1E-178, p-value ^{GC} = 1E-183) as well as regions surrounding internal exons (300 bp upstream to 100 bp downstream; p-value ^{TATA} = 1E-14, p-value ^{CCAAT} = 1E-14, p-value

^{GC} = 1E-5). This data indicated that regions immediately upstream of novel genic TSCs have typical promoter characteristics, validating their identity as TSSs.

Looking at the chromatin landscape surrounding the TSCs, we observed a consistent co-occurrence of enriched chromatin accessibility, H3K4me3, and H3K27ac around novel genic TSCs, indicating these TSCs were associated with an epigenetic signature characteristic of transcriptional activation (Figure 3F). On the other hand, we detected low signal for H3K4me1 and no signal for H3K27me3, which are typically found in enhancers and transcriptionally silent promoters, respectively. Additionally, we observed that the 5' signal at the closest annotated TSS was generally lower and hundreds of base pairs away from the RAMPAGE TSCs (Figure 3F). Complementarily, we analyzed these epigenetic marks in subgroups of novel genic TSCs determined by their genic location (exon, intron, intergenic, and promoters), which showed chromatin accessibility, H3K4me3, and H3K27ac enrichment in all subgroups (Figure S4, Supplementary material). Overall, the analyzed epigenetic information obtained from chromatin accessibility assays (ATAC-Seq) and chromatin immunoprecipitation assays (ChIP-Seq) from twelve of the analyzed biological samples, indicated that the novel TSCs associated with known genes represented functional TSSs.

For the TSCs that originated in exons of annotated genes, a substantial number of novel TSCs demonstrated low epigenetic signal, especially for H3K4me3, suggesting they could represent artifacts produced by RNA degradation or incomplete cDNA synthesis. By generating histograms of the epigenetic signal at these TSCs, we noted a bimodal distribution that separated TSCs into a group with higher epigenetic signal and a group with lower signal. By calculating the local minimum of epigenetic signal, we estimated that approximately 30% of the novel TSCs in exons fall into the latter group and could be potential artifacts (Figure S5).

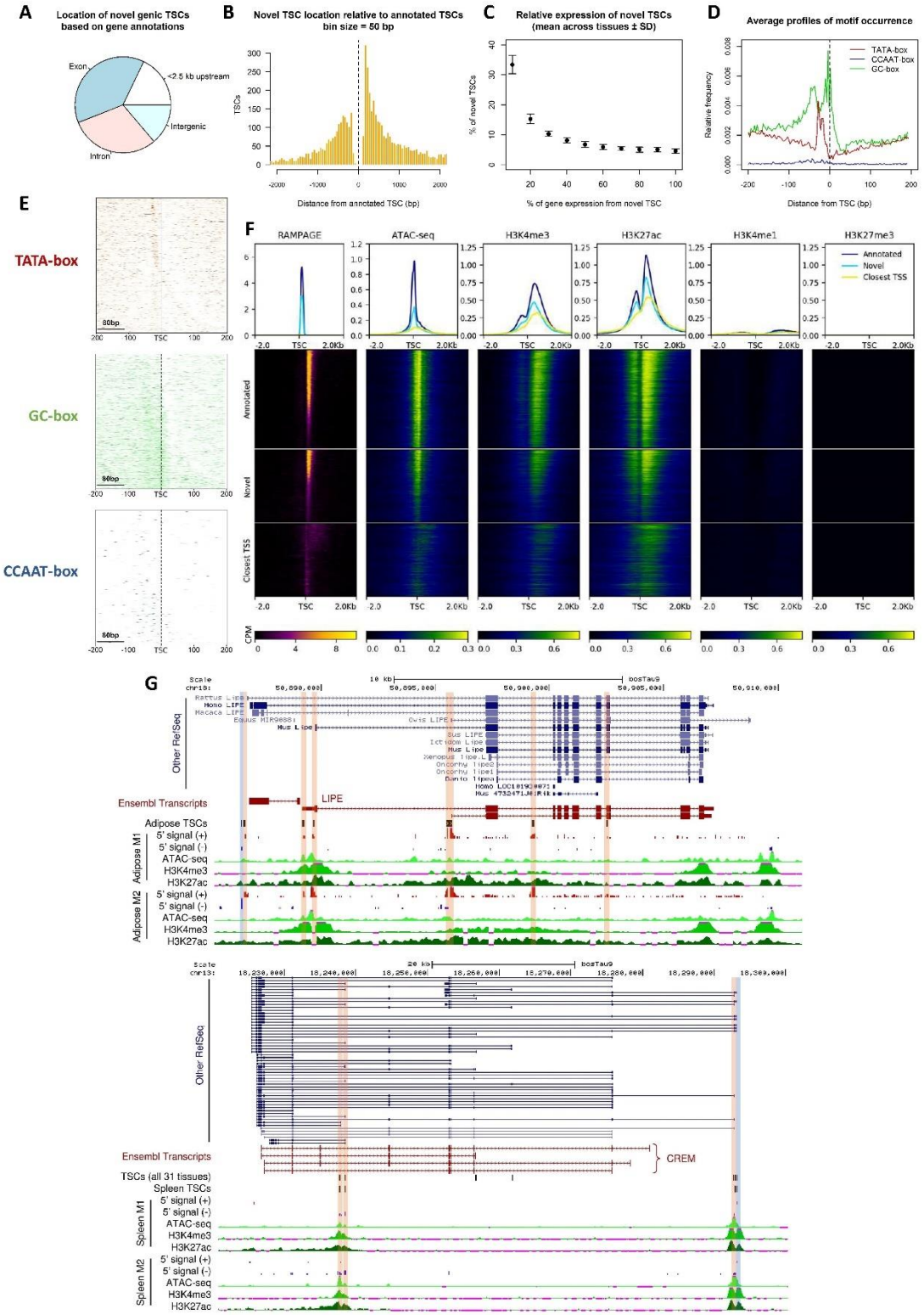
A
Location of novel genic TSCs based on gene annotations
Exon
<2.5 kb upstream
Intergenic
Intron
B
Novel TSC location relative to annotated TSCs bin size = 50 bp
TSCs
Distance from annotated TSC (bp)
C
Relative expression of novel TSCs (mean across tissues ± SD)
% of novel TSCs
% of gene expression from novel TSC
D
Average profiles of motif occurrence
TATA-box
CCAAT-box
GC-box
Relative frequency
Distance from TSC (bp)
E
TATA-box
GC-box
CCAAT-box
80bp
TSC
F
RAMPAGE
ATAC-seq
H3K4me3
H3K27ac
H3K4me1
H3K27me3
Annotated
Novel
Closest TSS
CPM
G
Other RefSeq
Ensembl Transcripts
LIPE
Adipose TSCs
Adipose M1
Adipose M2
5' signal (+)
5' signal (-)
ATAC-seq
H3K4me3
H3K27ac
CREM
TSCs (all 31 tissues)
Spleen TSCs
Spleen M1
Spleen M2

Figure 3. Novel promoters identified by RAMPAGE. (A) Location of novel TSCs according to gene annotations. (B) Histogram of the distance between novel TSCs and annotated TSCs. (C) Relative expression of novel TSCs. (D) Profiles of motif occurrence for TATA, CCAAT and GC-boxes around novel TSCs (± 200 bp). (E) Motif density maps for TATA, CCAAT and GC-boxes around novel TSCs (± 200 bp). TSCs are ordered ascendingly by size, i.e., upper rows represent narrow TSCs. The zero coordinate represents the 5' end of the TSC. Narrow TSCs were particularly enriched with TATA-box motifs and broad TSCs were enriched with GC-box motifs. (F) Epigenetic marks at reported and novel TSCs. The co-occurrence of chromatin accessibility and transcriptional activation marks (H3K4me3, H3K27ac) at novel TSCs, as well as the absence of poised enhancer and repressive marks (H3K4me1, H3K27me3), suggested these TSCs constituted promoter regions. The fuzzy signal observed around the closest annotated TSSs evidenced the absence of annotation for these novel elements. The data shown in the figure corresponds to the lung-M2 sample (>3 CPM). Heatmaps are colored according to CPM values. The remaining samples are available as supplementary material. (G) Novel TSCs for the *LIPE* and *CREM* genes. Most of the new variants are supported by annotations from other species. Antisense TSCs were marked with blue to distinguish them from sense TSCs (orange).

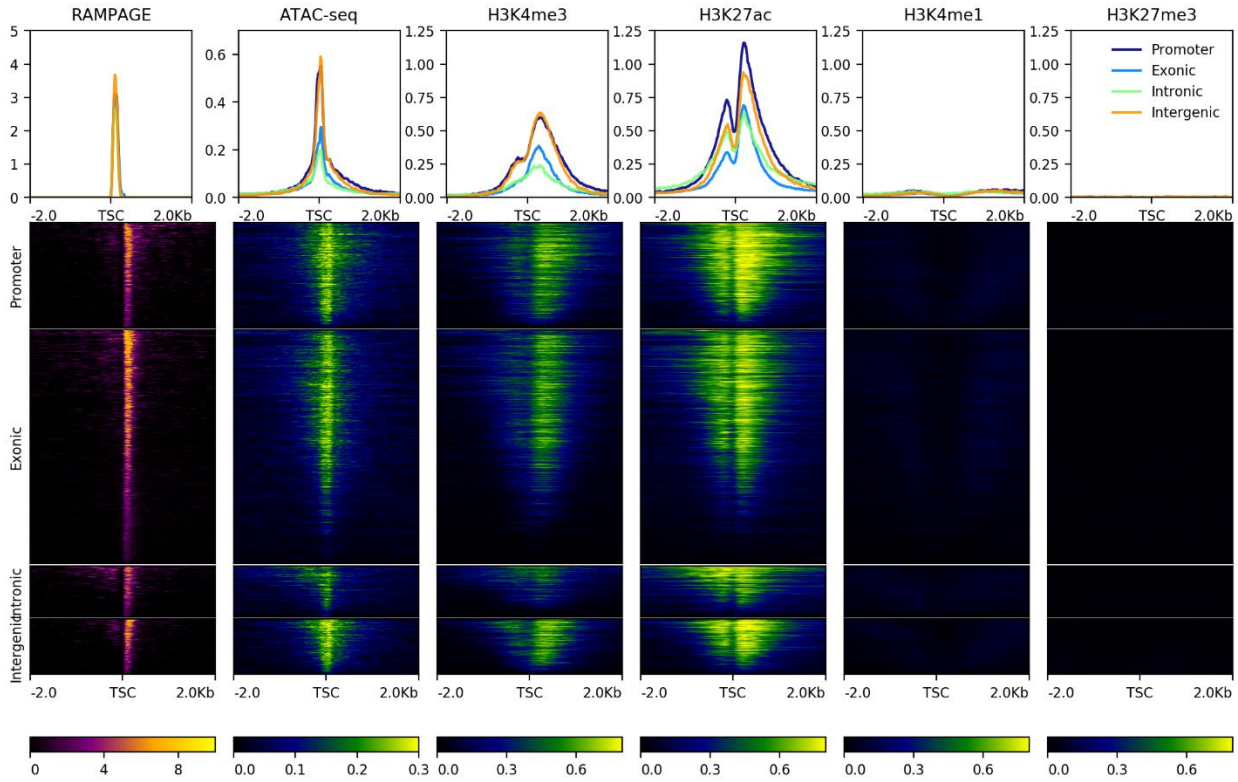

Figure S4. Epigenetic marks at subgroups of novel genic TSCs defined by their gene location (exon, intron, intergenic region, upstream of annotated TSS (promoter)) in the lung-M2 sample. A consistent co-occurrence of chromatin accessibility and transcriptional activation marks, as well as absence of poised enhancer and repressive marks, was observed in all subgroups. Heatmaps are colored according to CPM values. The remaining samples are available as supplementary material.

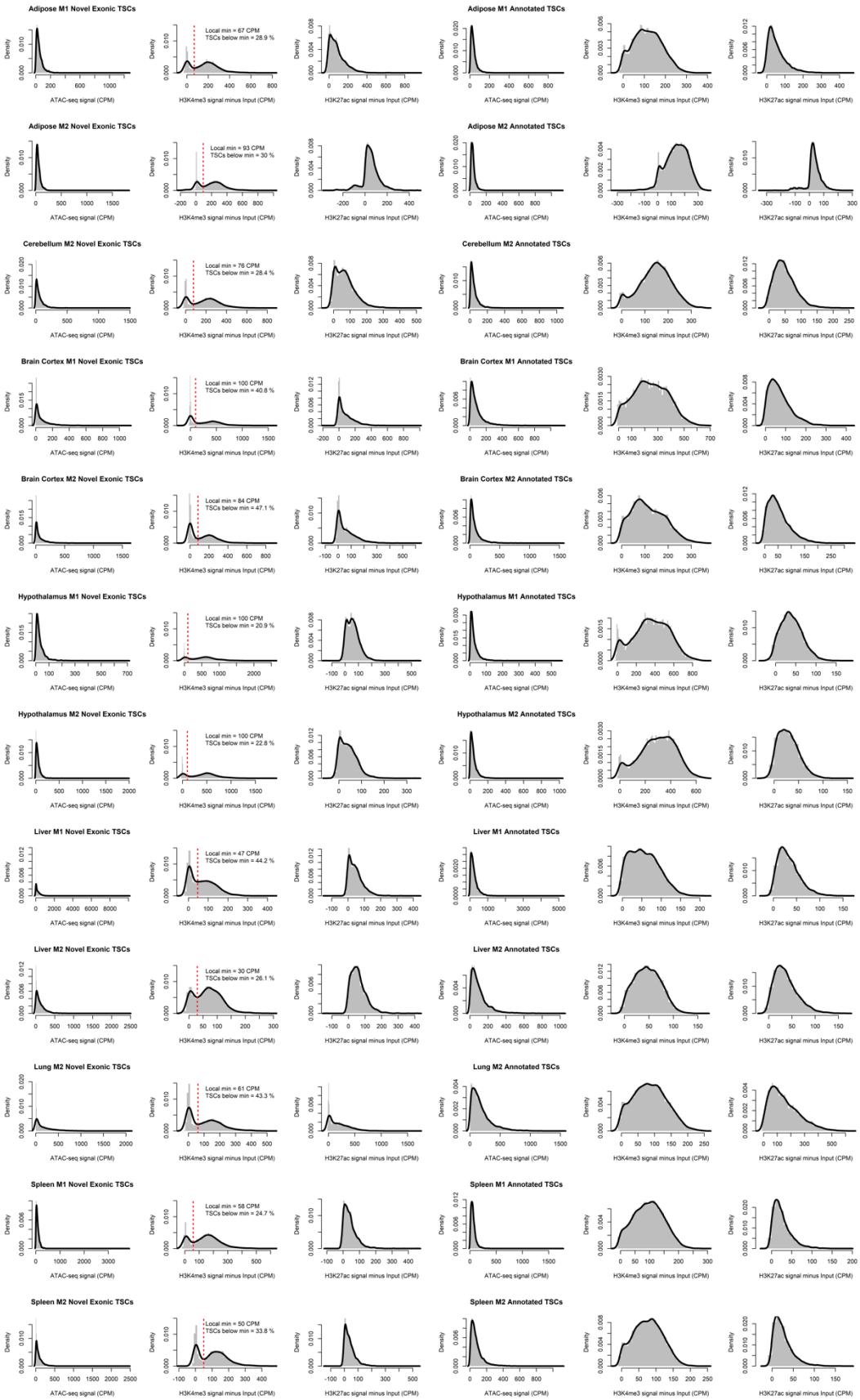
Adipose M1 Novel Exonic TSCs
Local min = 67 CPM
TSCs below min = 28.9 %
Adipose M1 Annotated TSCs
Adipose M2 Novel Exonic TSCs
Local min = 93 CPM
TSCs below min = 30 %
Adipose M2 Annotated TSCs
Cerebellum M2 Novel Exonic TSCs
Local min = 76 CPM
TSCs below min = 28.4 %
Cerebellum M2 Annotated TSCs
Brain Cortex M1 Novel Exonic TSCs
Local min = 100 CPM
TSCs below min = 40.8 %
Brain Cortex M1 Annotated TSCs
Brain Cortex M2 Novel Exonic TSCs
Local min = 84 CPM
TSCs below min = 47.1 %
Brain Cortex M2 Annotated TSCs
Hypothalamus M1 Novel Exonic TSCs
Local min = 100 CPM
TSCs below min = 20.9 %
Hypothalamus M1 Annotated TSCs
Hypothalamus M2 Novel Exonic TSCs
Local min = 100 CPM
TSCs below min = 22.8 %
Hypothalamus M2 Annotated TSCs
Liver M1 Novel Exonic TSCs
Local min = 47 CPM
TSCs below min = 44.2 %
Liver M1 Annotated TSCs
Liver M2 Novel Exonic TSCs
Local min = 30 CPM
TSCs below min = 26.1 %
Liver M2 Annotated TSCs
Lung M2 Novel Exonic TSCs
Local min = 61 CPM
TSCs below min = 43.3 %
Lung M2 Annotated TSCs
Spleen M1 Novel Exonic TSCs
Local min = 58 CPM
TSCs below min = 24.7 %
Spleen M1 Annotated TSCs
Spleen M2 Novel Exonic TSCs
Local min = 50 CPM
TSCs below min = 33.8 %
Spleen M2 Annotated TSCs
Density
ATAC-seq signal (CPM)
H3K4me3 signal minus Input (CPM)
H3K27ac signal minus Input (CPM)

Figure S5. ATAC-Seq, H3K4me3, and H3K27ac marks around novel TSCs in annotated exons (left) and known TSSs (right). The bimodal distribution of H3K4me3 signal allowed us to estimate that approximately 30% of the novel TSCs in annotated exons could be artifacts produced by incomplete cDNA synthesis or RNA degradation.

Unassigned TSCs

Many of the TSCs (n=44,125) showed no associations with any annotated lncRNA or protein coding genes, which could have surged as consequence of pervasive transcription (Wade and Grainger 2014). Pervasive transcripts are easily distinguished as they are non-coding, are not limited by gene boundaries, and are frequently antisense, so we proceeded to evaluate such aspects. Unassigned TSCs localized mainly to intergenic (58%) and intronic regions (38%), and were particularly abundant in the vicinity of genic TSCs, but on the opposite strand (Figure 4A), representing antisense RNA likely generated by bidirectional transcription (Engström et al. 2006). The search for antisense elements in regions 1.5 kb upstream and downstream of genic TSCs revealed 6,946 antisense TSCs associated with genic TSCs for 5,247 genes. Interestingly, 60% of these cases occurred within 500 bp upstream of genic TSCs (Figure 4B), which is consistent with previous observations in mouse (58%) (Lepoivre et al. 2013). Some of these antisense TSCs were highly correlated with their sense complements, suggesting they were regulated by the same promoter (Figure 4C). In terms of expression, antisense TSCs generally contributed substantially fewer transcripts than sense TSCs (Figure 4D). In addition to antisense TSCs in proximity to sense TSCs, we identified 6,342 antisense TSCs in gene bodies, resulting in 13,942 antisense TSCs in total, and accounting for 30% of the unassigned TSCs.

To further characterize the remaining unassigned TSCs, we generated partial transcript models (supplementary material) and predicted their coding potential based on k-mer frequencies,

codon usage, and open reading frame coverage. As a result, we identified 2,306 TSCs associated with potential lncRNAs and 259 TSCs associated with potential mRNAs (supplementary material). Lastly, we predicted pre-miRNA structures among the remaining models and identified 11,266 TSCs for candidate miRNA genes, which is slightly over the estimated number of human miRNA candidates (Alles et al. 2019). After identifying TSCs for potential mRNAs, lncRNAs, and pre-miRNAs, the number of remaining unassigned elements decreased to 18,259. The epigenetic marks at these loci showed unclear patterns (Figure S6), and the RAMPAGE signal failed to cluster samples by tissue (Figure S7), suggesting they represented technical artifacts. However, we could not discard the possibility that these TSCs corresponded to unannotated small RNAs or repetitive elements.

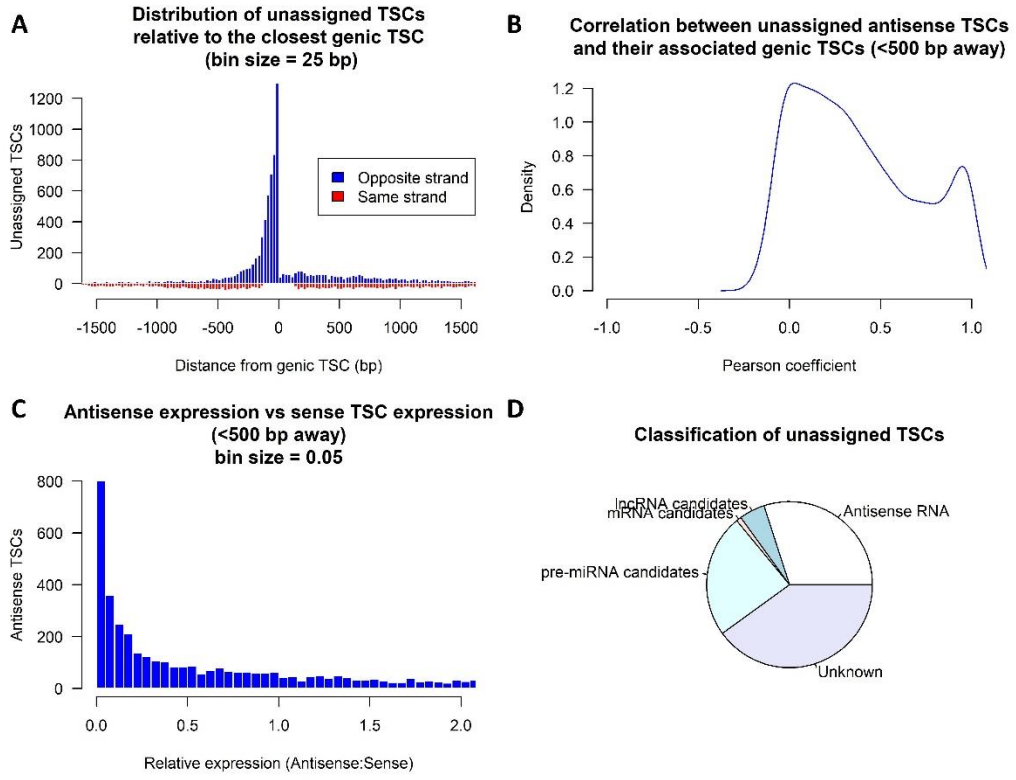

Figure 4. Identification of unassigned TSCs through bioinformatic approaches. (A) Distance between unassigned TSCs and the nearest genic TSCs. A high number of elements localized

within 500 bp upstream of genic TSCs but on the opposite strand. (B) Correlation of expression from antisense TSCs (CPM > 3) with expression from sense TSCs. (C) Expression of the antisense variant (CPM > 3) relative to the sense variant. (D) Putative roles attributed to unassigned TSCs.

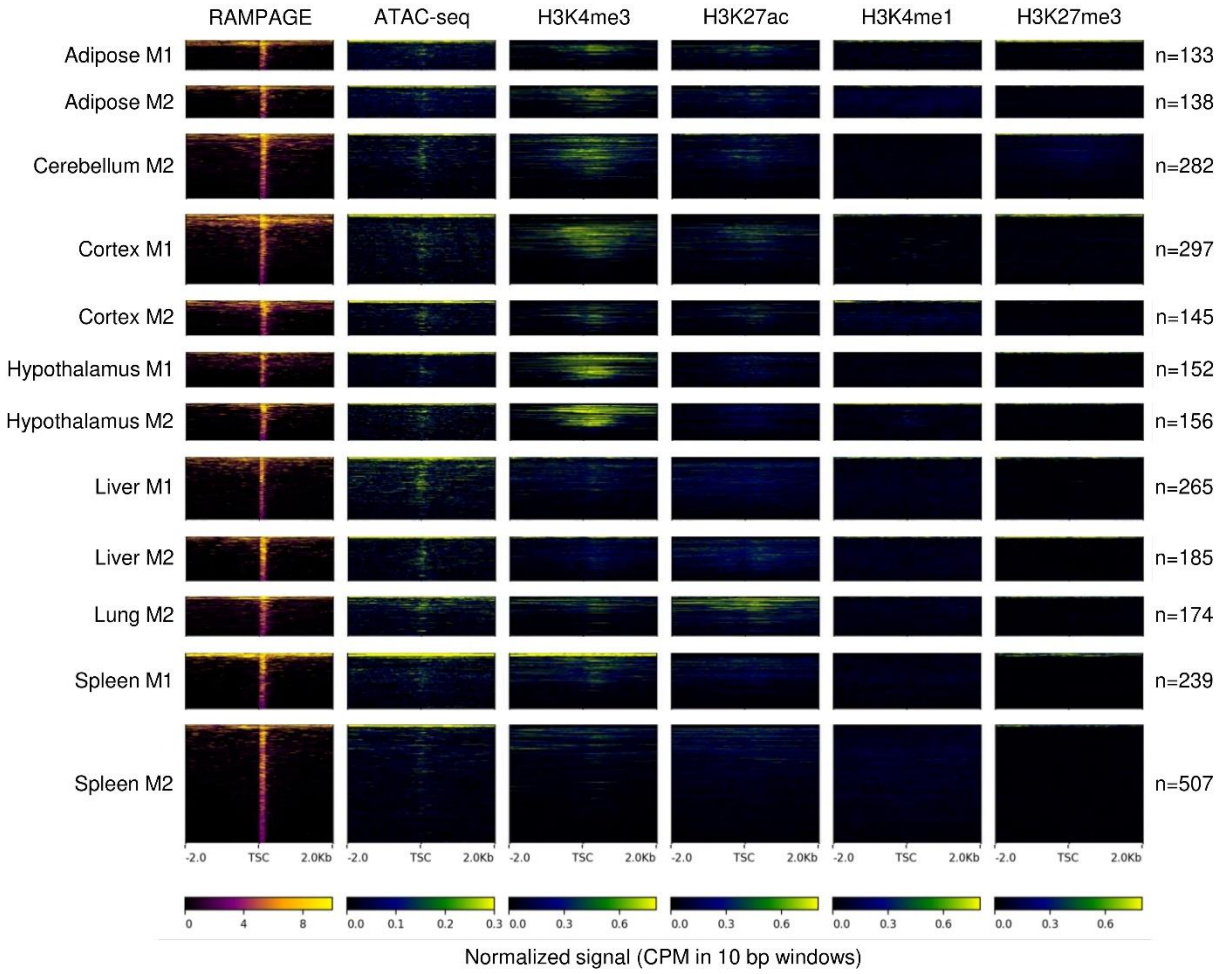

Figure S6. Epigenetic marks at the remaining unidentified TSCs. Patterns were unclear, suggesting these TSCs could have heterogeneous functions or constitute artifacts.

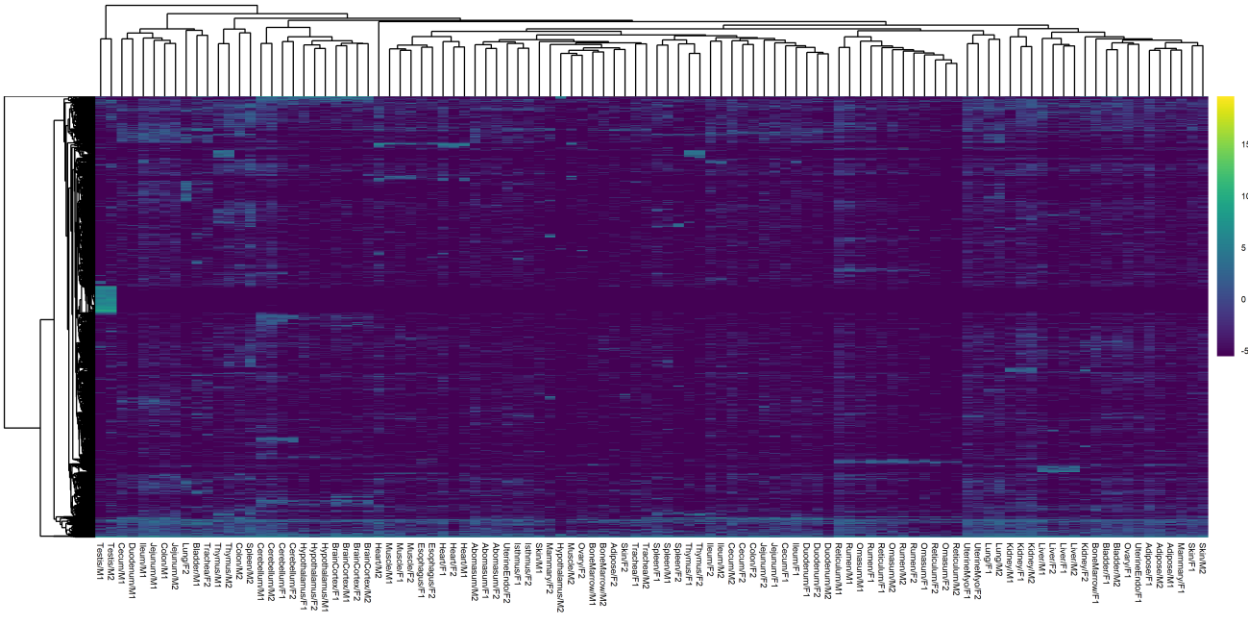

Figure S7. Hierarchical clustering based on RAMPAGE signal (variance-stabilized counts) at the remaining unassigned TSCs. Samples failed to cluster appropriately, suggesting many of these unassigned TSCs could be artifacts.

Analysis of promoter activity and specificity

Since RAMPAGE relies on the quantification of 5' signal coming from mature transcripts, the technique also provides useful information for gene expression and promoter activity studies. Making use of the 5' RAMPAGE signal, we conducted hierarchical clustering and principal component analyses (PCA) to evaluate the capacity of the methodology to capture differences in gene expression between tissues. Hierarchical clustering revealed patterns that reflected the diversity of transcriptional programs operating in our dataset (Figure 5A). Samples segregated according to tissue, system, and higher order structures, demonstrating that the method was quantitative enough to separate samples appropriately. Testis, brain, and muscle showed the most distinctive promoter activity profiles, as evidenced by the principal component analysis (Figure 5B).

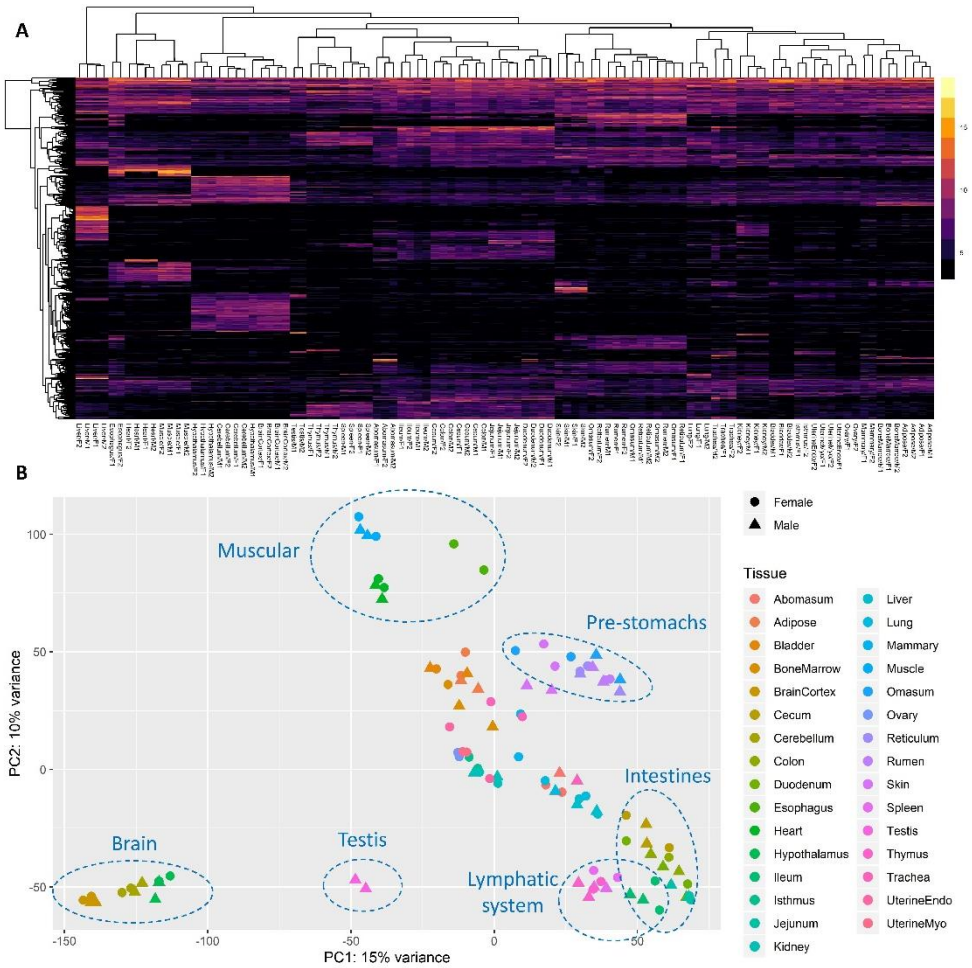

Figure 5. Promoter activity detected by RAMPAGE in 31 cattle tissues. (A) Heatmap representing transcriptional programs (variance-stabilized counts) in our tissue dataset. Samples clustered according to tissue and functionality. (B) Principal component analysis based on variance stabilized counts. Brain, testis, and muscular tissues showed very distinct profiles.

Based on the quantification of 5' signal in each sample, we generated an atlas with both genic and unassigned TSCs that will be helpful to track gene expression across bovine tissues (Table S2). To validate the RAMPAGE signal from a quantitative perspective, we compared RAMPAGE and conventional RNA-seq gene counts in seven tissues from the two male individuals. Estimates of gene expression by RAMPAGE were highly reproducible between

biological replicates (average Pearson R = 0.94, SD = 0.03) (Table S3, Figure S8), consistent with reproducibility of conventional RNA-seq (average Pearson R = 0.98, SD = 0.01) (Figure S9). Absolute quantification of gene expression was comparable between the two techniques (average Pearson R = 0.76, SD = 0.03) (Figures S10, S11), and detection of differentially expressed genes was strongly correlated between RNA-seq and RAMPAGE (average Pearson R = 0.9, SD = 0.05) (Figure S12). Overall, these results suggest slight differences in global transcriptome measurement by RAMPAGE and RNA-seq, although both assays captured highly similar levels of differential gene expression.

---Table S2 submitted as a separate file due to its size.---

Table S2. Promoter activity atlas. Location and expression (CPM) of each TSC (assigned and unassigned) in all samples. Counts were normalized with respect to the total number of fragments associated to TSCs in each sample.

RAMPAGE reproducibility		
Tissue	**Female**	**Male**
Abomasum	0.93	NA
Adipose	0.93	0.94
Bladder	NA	0.92
Bone marrow	NA	0.93
Brain cortex	0.96	0.96
Cecum	0.94	0.94
Cerebellum	0.97	0.98
Colon	NA	0.96
Duodenum	0.93	0.88
Esophagus	0.94	NA
Heart	0.95	0.95
Hypothalamus	0.93	0.91
Ileum	0.95	0.92
Isthmus	0.94	NA
Jejunum	0.94	0.95
Kidney	0.92	0.96
Liver	0.95	0.96
Lung	0.93	NA
Mammary gland	0.86	NA
Muscle	0.94	0.96
Omasum	0.92	0.92
Ovary	0.95	NA
Reticulum	0.94	0.93
Rumen	0.96	0.95
Skin	0.84	0.89
Spleen	0.94	0.96
Testis	NA	0.96
Thymus	0.94	0.96
Trachea	0.91	NA
Uterine endometrium	0.89	NA
Uterine myometrium	0.96	NA

RNA-Seq reproducibility	
Tissue	**Male**
Adipose	0.98
Cerebellum	0.97
Brain cortex	0.98
Hypothalamus	0.97
Liver	0.97
Lung	0.98
Muscle	0.97
Spleen	0.98

Table S3. Reproducibility of gene expression between RAMPAGE and RNA-Seq replicates. Based on Pearson correlations, estimates of gene expression by RAMPAGE were highly reproducible between biological replicates, consistent with reproducibility of conventional RNA-seq.

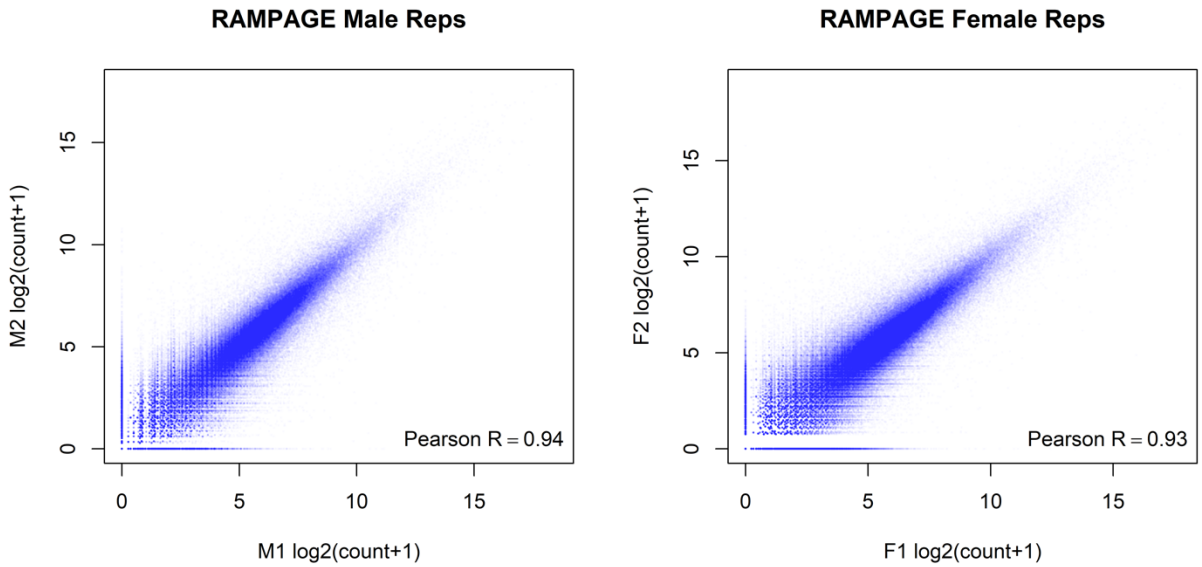

Figure S8. Reproducibility between RAMPAGE replicates. Counts were normalized by DESEQ2.

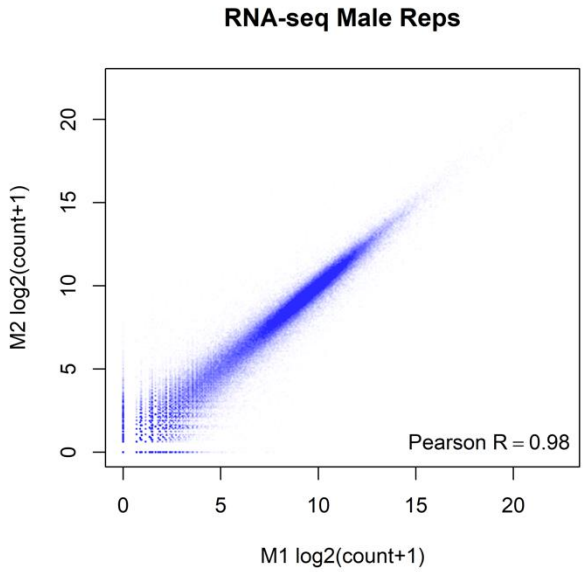

Figure S9. Reproducibility between replicates for RNA-Seq counts. Counts were normalized by DESEQ2.

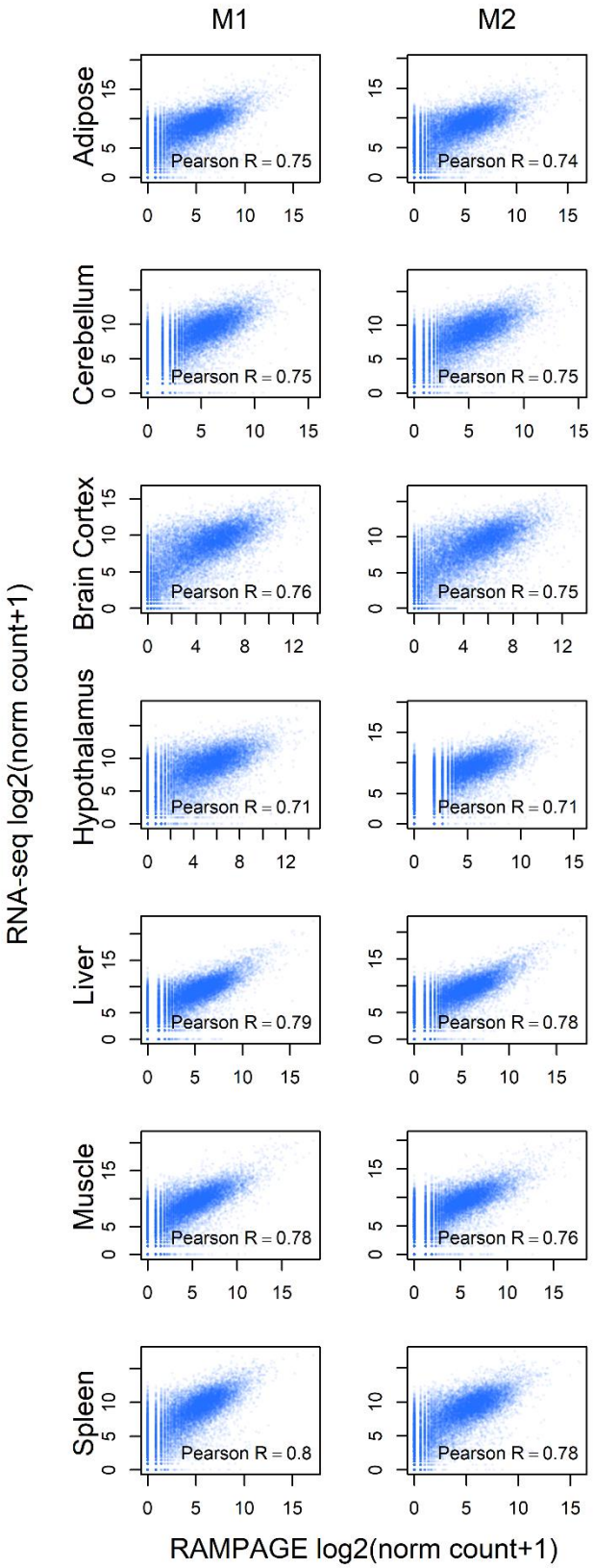

Figure S10. Pairwise correlations between RNA-Seq and RAMPAGE log-transformed normalized counts. Moderately high correlations were consistently observed across samples. Counts were normalized by DESEQ2.

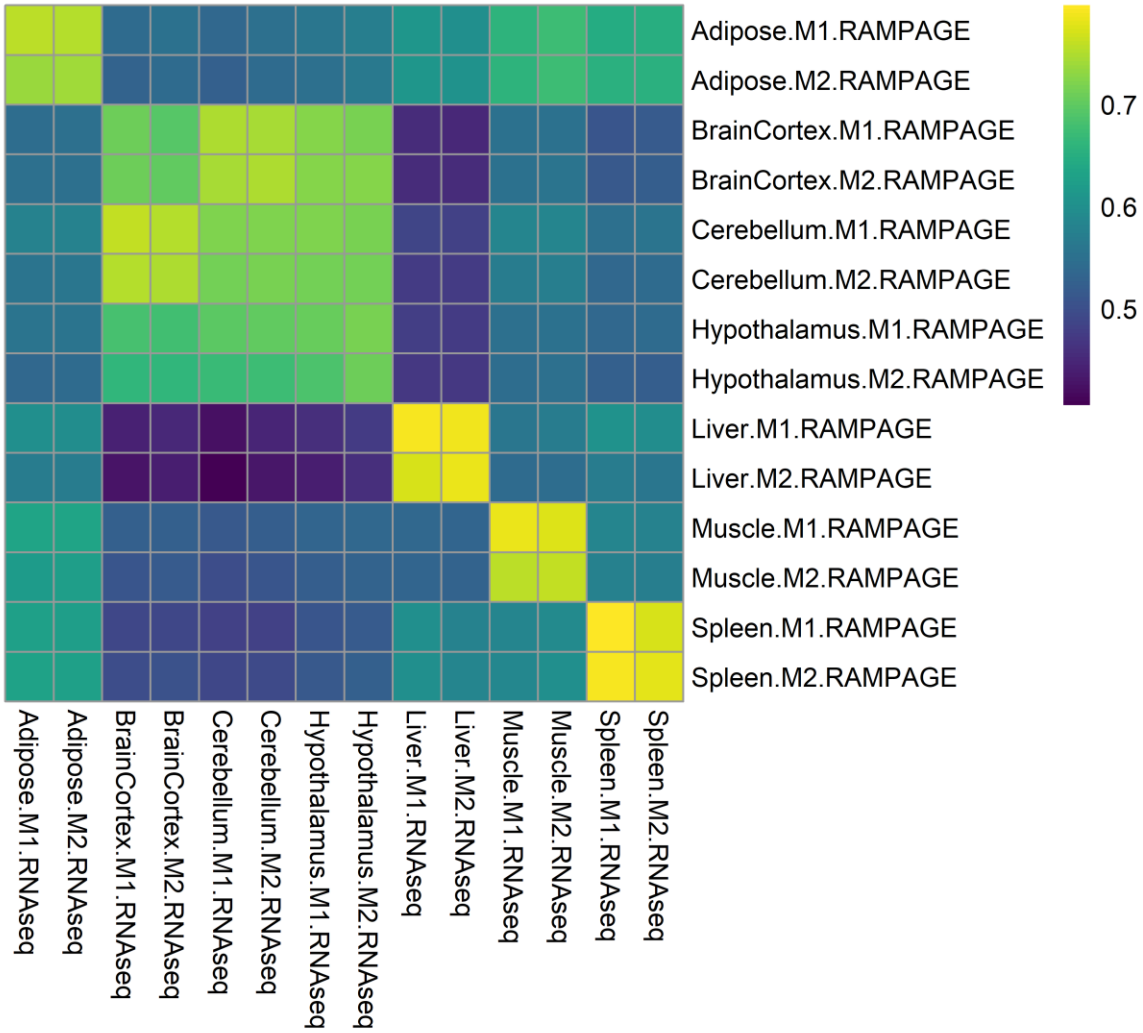

Figure S11. Pearson correlation between RNA-Seq and RAMPAGE log-transformed normalized counts. High correlation was observed between samples from the same tissue. Counts were normalized by DESEQ2.

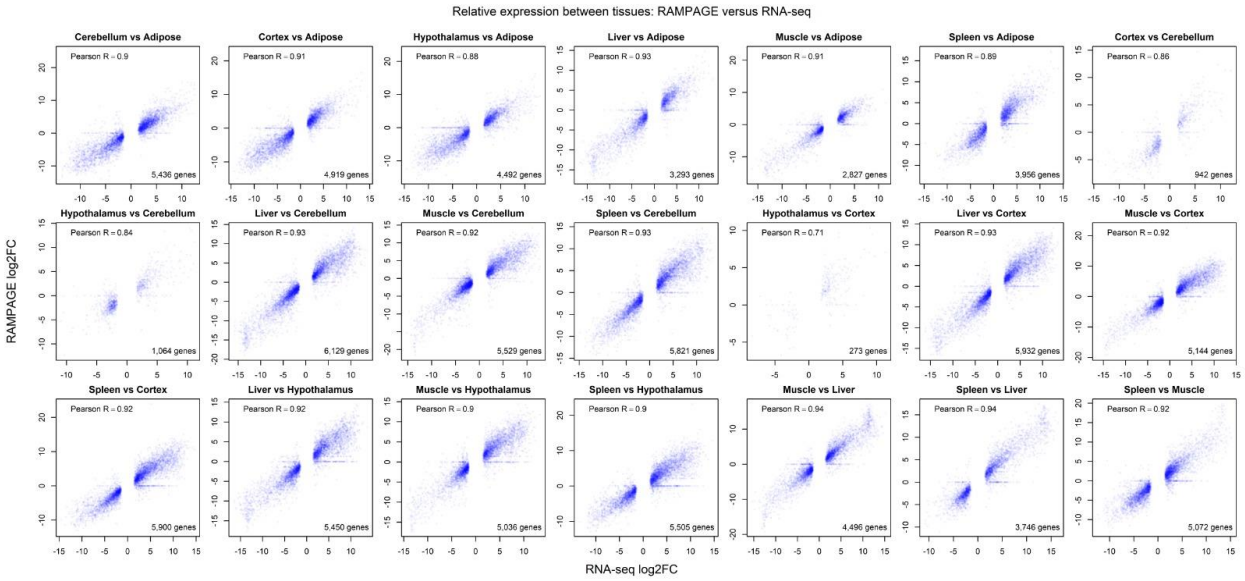

Figure S12. Pairwise correlations between logFC values obtained from RNA-Seq and RAMPAGE gene counts. The analysis contemplates differentially expressed genes first identified by RNA-Seq. Correlations were high except for brain tissues, where differences in gene expression were minimal.

Expression profiles from alternative TSCs of the same gene were generally independent, as evidenced by the low correlation coefficients obtained in pairwise comparisons (Figure 6A). This observation suggested alternative TSCs were likely regulated by different biological mechanisms, while a small proportion of alternative TSCs seemed to be controlled by the same regulator.

To identify groups of co-regulated transcripts and study their tissue-specificity, we generated co-expression networks. We found 34 modules of co-expressed TSCs with different degrees of tissue-specificity (Figure 6B, Table S4), which varied from single tissues to high-level structures, such as brain or digestive epithelium (Figures 6C, 6D). The largest module corresponded to testis and comprised 6,854 TSCs, followed by brain (3,194 TSCs), and intestines (1,888 TSCs).

These numbers are consistent with studies in human and mouse, which have demonstrated that the testis expresses the largest number of tissue-specific genes (over twice as many as the second ranked tissue, brain cortex) (Djureinovic et al. 2014; Guo et al. 2005).

---Table S4 submitted as a separate file due to its size.---

Table S4. Genic TSCs and their corresponding co-expression modules.

Promoters from each module were significantly enriched in binding motifs for transcription factors associated with their respective tissues (Figure S13). For instance, the Esophagus-Heart-Muscle module was enriched in binding motifs for all members of the myocyte enhancer factor-2 (*MEF2*) family, which are known to regulate muscle specific genes and muscle development (Gossett et al. 1989).

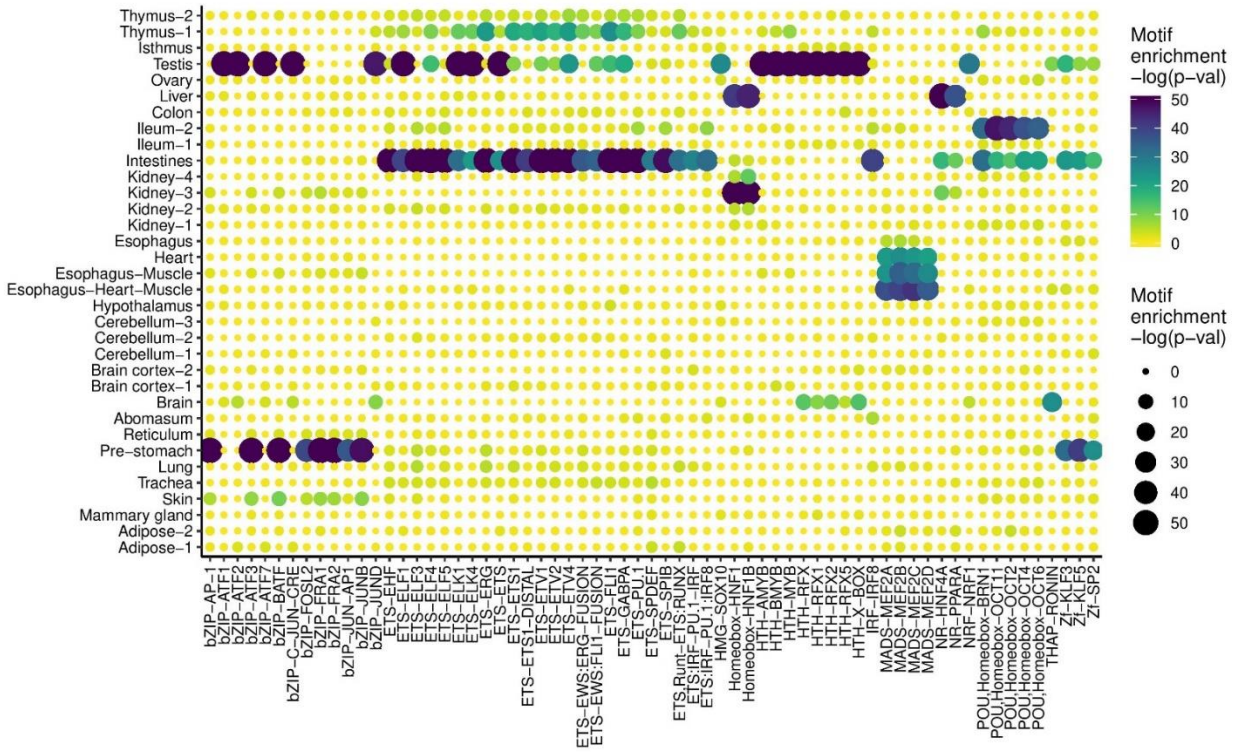

Figure S13. Binding motif enrichment in regions from 300 bp upstream to 100 bp downstream of co-expressed TSCs. Networks were enriched in binding motifs representative of their tissues.

The identification of tissue-specific TSCs allowed us to analyze the use of alternative promoters across tissues: we analyzed 3,336 genes detected in at least two co-expression modules and found 601 genes whose transcripts originated from alternative promoters in either testis or brain, which represented the highest use of alternative promoters between pairs of modules (Figure 6E, 6F, 6G). The gene ontology (GO) analysis of these genes revealed a significant enrichment in terms related to cytoskeleton components, microtubule binding, ATP-binding kinase activity, synapse, cell-cell adhesion, microtubule-based movement and transport, and kinesin activity (Table S5). We also found statistical enrichment in synapse pathways, including GABAergic synapse, cholinergic synapse, glutamatergic synapse, and serotonergic synapse, as well as critical pathways from the hypothalamus-pituitary-gonad (HPG) axis, such as GnRH and GABA

signaling. The high number of members and use of alternative promoters found in these two tissues evidenced the complexity they acquired throughout evolution. Following the testis-brain combination, we found testis-intestines, with 357 genes, and testis-liver, with 325 genes using alternative promoters in each tissue. Genes shared by testis and intestines were highly enriched in GO terms related to cell cycle and division control, GTPase activity regulation, kinase activity, and additional groups of processes with lower enrichment (Table S5). Genes shared by testis and liver, on the other hand, were slightly enriched in terms related to acyl-CoA-binding, mitochondrial components, and steroid and lipid metabolism (Table S5).

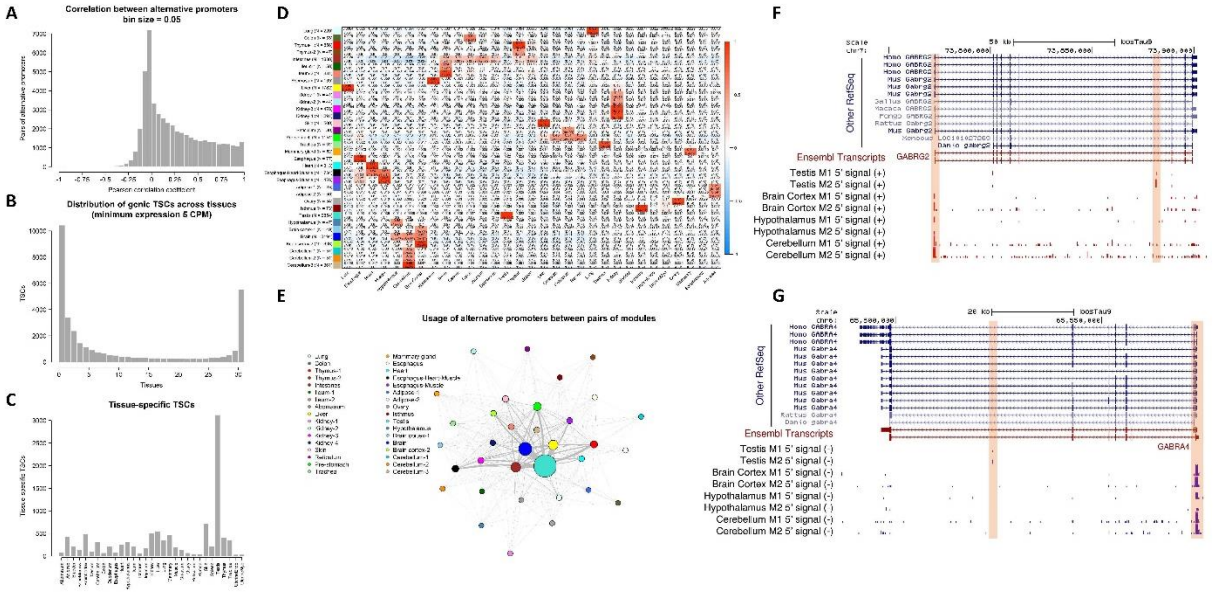

Figure 6. Usage of promoters across bovine tissues. (A) Correlation between pairs of alternative TSCs from the same gene (>5 CPM). We found that alternative TSCs were generally independent from each other. (B) Usage of TSCs across tissues. Some of the TSCs were active in all tissues, but the majority was active in only a few of them. (C) Tissue-specific TSCs identified in our dataset. Testis showed a high number of tissue-specific elements. (D) Networks of TSC co-expression including Pearson correlations to each tissue and their p-values. (E) Use

of alternative TSCs between pairs of tissues. The size of the sphere represents the number of TSC members that the module contains, while the thickness of the connection represents the number of common genes expressed from different (tissue-specific) TSCs. (F, G) Examples of the use of tissue-specific promoters between brain and testis. The *GABRG2* and *GABRA1* genes are members of the GABAergic synapse pathway.

---Table S5 submitted as a separate file due to its size.---

Table S5. Functional annotation clustering of genes shared by the testis and brain co-expression modules.

DISCUSSION

In this study, we analyzed a large collection of bovine tissues from both sexes using the RAMPAGE approach, identifying thousands of TSCs associated with protein coding and lncRNA genes. The diversity of analyzed tissues captured the expression of 18,312 previously annotated genes. However, no expression was detected for 5,016 genes, likely reflecting the fact that all tissues were from adult animals and lacked expression of developmentally associated genes. Thus, an additional analysis of samples at different stages of development should be performed to generate an even more comprehensive TSS annotation of the bovine genome.

Our dataset allowed us to identify several known and novel TSCs with a broad range of sizes. Size variation was expected as mammalian promoters are known to allow transcription to start from both well-defined positions (TATA box-enriched promoters) and broad intervals (CpG-rich promoters) (Carninci et al. 2006). In fact, we found that regions upstream of narrow TSCs were

enriched with TATA-box elements, whereas regions upstream of broad TSCs were enriched in GC-box and CCAAT-box elements. In addition, novel TSCs were supported by experimental evidence that revealed the presence of chromatin accessibility and transcriptional activation marks (H3K4me3, H3K27ac) and the near absence of H3K4me1, an epigenetic mark historically used for enhancer annotation (Heintzman et al. 2007), which implicated these novel TSCs as part of promoters. In addition to TSCs associated with annotated genes, we found many unassigned TSCs that supported the existence of pervasive transcription. A considerable number of unassigned TSCs were upstream of genic TSCs and seemed to be a consequence of bidirectional promoter activity. As shown in mouse (Lepoivre et al. 2013), transcripts from bidirectional promoters were more correlated to each other than transcripts from alternative TSCs of the same gene, suggesting a common regulatory mechanism. Furthermore, antisense transcripts presented low expression levels in comparison to their complementary sense transcripts, supporting the concept of pervasive transcription by erratic behavior of the polymerase.

Even though the RAMPAGE method has important advantages over other 5'-seq techniques for TSC identification (Adiconis et al. 2018), including CAGE due to extensive use of paired-end information (Batut et al. 2013), false TSCs were expected to arise as products of incomplete cDNA synthesis and mRNA degradation. We estimated that about 30% of the 13,209 novel TSCs in annotated exons could be false positives as shown by the low H3K4me3 signal. However, due to the low number of tissues with epigenetic information in comparison to the RAMPAGE dataset, our evidence was insufficient to identify and discard all potential artifacts. A global estimation based on the assumptions that artifacts are most frequent in exons (downstream of the strongest TSC), expressed to a lower extent (< 25%), and correlated to the strongest TSC for being part of the same transcript (Pearson > 0.5), suggested that 4,059 (8.7%) of the genic TSCs could be false, and also supported the initial estimation by epigenetic

signal in the reduced dataset. However, the identity of these sites needs to be corroborated with additional epigenetic information from other tissues.

The analysis of co-expression networks revealed a high number of genes expressed in both brain and testicle under different tissue-specific TSCs. The high similarity between brain and testis expression profiles was reported years ago in mouse and human (Guo et al. 2005, 2003). The mechanisms and epigenetic factors contributing to the projection of the brain expression program on the testis are unclear, although intriguing. It has been proposed that the hypothalamus-pituitary-gonad (HPG) could be implicated in the maintenance of this similarity, given the importance of the brain expression program for human speciation and transmission to the offspring (Guo et al. 2005). Our study, however, demonstrated that although brain and testis share a high number of genes, transcripts are expressed from tissue-specific promoters. These promoters could be generating isoforms with different and unique functions. This information could be valuable to understand the regulatory mechanisms operating behind tissue-specific expression programs.

With our set of new TSCs, the bovine ratio of TSS to genes reached a level comparable to the human and mouse genomes. Hopefully, this addition to the annotation will be of use for the cattle research community, and for future studies regarding gene expression from alternative promoters and conservation of transcriptional regulation between species.

METHODS

Sample collection

Samples from abomasum, adipose, bladder, brain cortex, bone marrow, cecum, cerebellum, colon, duodenum, esophagus, heart, hypothalamus, ileum, isthmus, jejunum, kidney, liver, lung, skeletal muscle, mammary gland, omasum, ovary, reticulum, rumen, skin, spleen, testis,

thymus, trachea, uterine endometrium and uterine myometrium were collected from two female and two male Line 1 Herefords provided by Fort Keogh Livestock and Range Research Lab at 14 months of age. Sample collection was carried out with all the necessary permissions, following Protocol for Animal Care and Use #18464, approved by the Institutional Animal Care and Use Committee (IACUC), University of California, Davis. Cattle were slaughtered by captive bolt under USDA inspection at the University of California, Davis. Collected tissue samples were flash frozen in liquid nitrogen and stored at −80 °C until processing.

RAMPAGE library preparation

Frozen tissues kept at -80°C were homogenized with a mortar and pestle in liquid nitrogen. Total RNA was extracted using Trizol (Invitrogen, Carlsbad, CA) followed by a column clean-up using the Direct-zol RNA Mini Prep Plus kit (Zymo Research, Irvine, CA) and performing an in-column DNA digestion. Integrity of the DNase-treated RNA was verified on the Experion electrophoresis system (Bio-Rad, Hercules, CA). The RNA quality indicator (RQI) varied from 7.5 to 9.7, indicating good quality RNA, excepting Liver from Male A which had a borderline RQI of 6.9.

Following the method described by Batut & Gingeras, (2013), DNase-treated RNA was subjected to terminator digestion (TEX enzyme, Epicentre) to degrade 5'-monophosphate RNA (16S and 18S ribosomal RNA). Random primers bearing an adapter sequence overhang were annealed to the RNA, which was then subjected to reverse transcription, leaving a string of terminal cytosines. Template–switching oligonucleotides (TSO) containing the library identification barcodes were then hybridized to these terminal cytosines, prompting the reverse transcriptase to switch templates and add the TSO sequence to the end of the newly synthesized cDNA. The TSO bears an Illumina adaptor sequence, such that only 5’-complete cDNAs are amplifiable, whereas non-5’ complete molecules are not. Libraries were then quantified by qPCR to pool multiple samples for sequencing.

Libraries were pooled in equimolar amounts and 5’ caps were oxidized with sodium periodate. To prepare for cap trapping, 5’caps were biotinylated, and RNA molecules were pulled down using streptavidin magnetic beads. Finally, pooled libraries were PCR-amplified and size-selected using AmPure XP magnetic beads. Final pooled libraries were quantified in the Nanodrop spectrophotometer (Thermo Scientific, Wilmington, DE, USA) and the Bioanalyzer 2100 High-Sensitivity DNA chip (Agilent Technologies, Santa Clara, CA, USA). Libraries had the expected size range of 300 to 1000 bp, and were sequenced on an Illumina HS 4000 system, generating paired end reads of either 100 or 150 bp.

RNA-seq data analysis

Data for RNA-seq (Kern et al. 2018) were downloaded from the European Nucleotide Archive, project ID PRJEB14330 (https://www.ebi.ac.uk/ena/data/view/PRJEB14330). Reads were trimmed using Trimmomatic (v0.33) to remove Illumina sequencing adapters and low-quality bases. Settings for adapter removal included a maximum of two mismatches, a palindrome clip threshold of 30, and a simple clip threshold of 10. Leading and trailing bases of quality less than 3 were removed. Sliding window trimming was conducted using a window size of 4 and minimum average quality of 15. After processing, reads shorter than 36 bp were discarded. Samples were aligned to the ARS-UCD1.2 Bos taurus reference genome using STAR v2.6.1 (Dobin et al. 2013) with options --outFilterScoreMinOverLread 0.85 and --seedSearchStartLmax 30.

RAMPAGE data analysis

Samples were aligned to the ARS-UCD1.2 Bos taurus reference genome using STAR in two-pass mode. The first six nucleotides of the first read (barcodes) were removed prior to alignment as part of the demultiplexing step. The last 15 nucleotides of the second read corresponded to the RT-primer, thus they were soft-clipped using the --clip5pNbases option during the alignment

step. Only uniquely mapped reads were kept for subsequent analyses. In order to improve the specificity of the peak calling and the accuracy of transcript quantification, duplicates were marked and removed based on the alignment coordinates and the last 15 nucleotides of the second read (random primer), which were used as a pseudo-random single-molecule barcode to distinguish true duplicates. Alignments from the same sample were merged prior to peak calls. A preliminary assessment of data quality was carried out using hierarchical clustering of gene counts generated by featureCounts v1.6.2 (Liao et al. 2014) prior to peak calling. Samples showing anomalous expression profiles compared to other biological replicates from the same tissue were discarded from subsequent analyses.

RAMPAGE peak calling

The 5' coordinate of each cDNA was recorded and compiled into a single wiggle file as a quantification of every possible TSS in the dataset. Then, the same was done for every genomic position covered by downstream reads to create a signal background for the peak calling algorithm. Peak calling was conducted using the algorithm developed by Batut et al. (2013) with a dispersion parameter of 4, a background weight of 0.6, and an FDR of 1E-8 in the combined dataset. Briefly, the algorithm works as a sliding window that, for each position in the genome, assesses the statistical enrichment of 5' signal against a negative binomial background distribution. The coverage by downstream reads in such window is used to subtract a pseudo-count from the 5' signal so that significance is harder to achieve at highly transcribed exon positions. Then, neighboring windows are merged and trimmed at the edges down to the first base with signal. The script is available as supplementary material (RAMPAGEpeakCaller.py).

To increase the sensitivity for tissue-specific (weak) peaks, each tissue was also analyzed separately using a dispersion parameter of 0.2, a background weight of 0.8, and an FDR of 1E-8. Tissue-specific TSCs undetected in the combined dataset, supported by at least 3

independent RAMPAGE tags, located outside exons, and conserved in at least two biological replicates, were incorporated into the global list of TSCs.

Gene assignment

TSCs were assigned to genes using featureCounts in stranded mode (-s 1) and the Ensembl v95 annotation. Gene associations supported by less than three independent fragments were considered weak associations. To exclude spurious associations generated by run-off transcription, i.e. transcription that failed to terminate at the right site and continued over a downstream gene, associations to alternative genes supported by 5-fold fewer reads than the most supported gene were disregarded. For quantification purposes, the RAMPAGE signal was normalized by library size (total number of reads associated with TSCs). Genes were considered as expressed when their expression (normalized with respect to all the RAMPAGE tags assigned to genes) reached a minimum of 3 counts per million (CPM).

Expression quantification by RNA-seq and RAMPAGE

For RAMPAGE, gene expression was quantified using the number of 5' tags in TSCs attributed to genes. Genes with less than 10 total counts across all samples were removed from the analysis prior to normalization to eliminate background noise. Gene counts were normalized by DESeq2 (Love et al. 2014). Normalized counts were log-transformed and used to calculate Pearson correlations between biological replicates for each tissue. Log-transformed normalized counts from all tissues were then pooled to calculate the overall Pearson correlations between male replicates in all tissues and female replicates in all tissues.

For comparison, gene expression was also evaluated from RNA-seq data for a subset of seven tissues. For RNA-seq, raw expression values for genes in the Bos taurus annotation (Ensembl v95) were calculated from uniquely mapped reads using the SummarizeOverlaps function from the GenomicAlignments R package (Lawrence et al. 2013) with the 'union', paired-end, and

stranded options. Genes with less than 10 total counts across all samples were removed from the analysis prior to normalization to eliminate background noise. Gene counts were then normalized by DESeq2 and log-transformed. Log-transformed normalized counts from all seven tissues were pooled to calculate the overall Pearson correlation between male replicates. For the seven tissues for which RNA-seq data were available, log-transformed normalized counts were used to calculate Pearson correlations between RNA-seq and RAMPAGE. Finally, differential gene expression was compared between RNA-seq and RAMPAGE. From RNA-seq counts, differentially expressed genes (DEG) were identified for each pair of tissues using DESeq2 and lfcShrink (type="apeglm", lfcThreshold=1), given an s-value < 0.005. The log fold change (logFC) of these DEG were then calculated by DESeq2 according to RNA-seq and RAMPAGE data and used to calculate Pearson correlations.Correlations were calculated and visualized using custom scripts and built-in functions in R.

ATAC-Seq and ChIP-Seq data analysis

Data for ChIP-Seq (Kern et al. 2018) and ATAC-Seq assays were downloaded from the European Nucleotide Archive, project ID PRJEB14330 (https://www.ebi.ac.uk/ena/data/view/PRJEB14330). ATAC-seq reads were trimmed with trim_galore! v0.4.0 (github.com/FelixKrueger/TrimGalore) (-q 20 -a CTGTCTCTTATA -stringency 1 –length 10) and aligned to the ARS-UCD1.2 genome with BWA mem (Li and Durbin 2009). Duplicate alignments were removed using Picard Tools v2.9.1 (broadinstitute.github.io/picard). Low-quality alignments (q < 15) were removed with SAMtools v1.9 (Li et al. 2009). ChIP-seq reads were processed following the original study (Kern et al. 2018)**.** To visualize signal, the bamCoverage function of the deepTools v3.2.0 software (Ramírez et al. 2016) was used to calculate normalized coverage (CPM) in 10 bp windows genome-wide. For ChIP-seq, signal from input libraries was first subtracted with deepTools bigwigCompare. Normalized signal from ATAC-seq and ChIP-seq libraries was plotted

alongside RAMPAGE 5' signal on the UCSC genome browser. The deepTools computeMatrix and plotHeatmap functions were also used to plot normalized epigenetic signal at TSCs, plotting the median signal above heatmaps and using the interpolation method "bilinear" for smoothing. The average epigenetic signal (CPM) at TSC was calculated with the bigWigAverageOverBed function from the UCSC Genome Browser utilities. Pearson correlations comparing epigenetic signal and RAMPAGE signal at TSCs were calculated and visualized using custom scripts and built-in functions in R.

Identification of binding motifs

The abundance of TATA, GC and CCAAT boxes in regions 200 bp upstream to 200 bp downstream of novel TSCs was visualized using the seqPattern R package (https://bioconductor.org/packages/release/bioc/html/seqPattern.html). The search was carried out using the TATA-binding protein (Tbp) model included in the package, the MA0079.2.pfm JASPAR model for specificity protein 1 (Sp1) and the MA0060.3.pfm JASPAR model for nuclear transcription factor Y (Nfy).

Statistical enrichment was evaluated using the 'findMotifsGenome.pl' tool from HOMER v4.10.4 (Heinz et al. 2010). Background consisted of either random sequences from the rest of the genome or sequences from the rest of the gene body depending on the location of the TSC evaluated (promoters and intergenic regions, or exons and introns, respectively). The search was conducted on sequences 300 bp upstream to 100 bp downstream of the TSCs using binding motifs for Tbp, Sp1 and Nfy available in the HOMER database.

Attribution of unassigned TSCs

Unguided partial transcript models were generated for RNAs derived from unassigned TSCs using Stringtie v2.0.4 (Pertea et al. 2015) in --fr stranded mode, a minimum isoform fraction of 0, a minimum assembled transcript length of 30, a minimum of one read per bp coverage, and

trimming based on coverage disabled. Antisense RNAs mapping to the gene body were identified using featureCounts in the opposite stranded mode (-s 2). Putative protein coding and lncRNA genes were predicted based on k-mer frequency, codon use, and ORF coverage using the FEELnc software (Wucher et al. 2017). Lastly, prediction of pre-miRNA candidates was carried out using the miRNAfold tool (Tav et al. 2016) with a sliding window size of 60 bp and FASTA files containing the remaining partial transcripts as input.

Evaluation of alternative promoter usage

Correlations between alternative TSCs from the same gene were evaluated considering highly expressed genic TSCs (>5 CPM normalized with respect to the number of RAMPAGE tags assigned to genic TSCs) through the Pearson coefficient.

The use of alternative promoters was analyzed through signed co-expression networks generated by the WGCNA R package (Langfelder and Horvath 2008). To reduce noise, networks were constructed for TSCs with a minimum expression of 3 CPM in at least two samples of any tissue. The adjacency matrix was generated using variance-stabilized counts as input, biweight mid-correlations and a soft-thresholding power of 12. Modules were determined using the Dynamic Hybrid Tree Cut algorithm with a sensitivity (deepSplit) of 2 and PAM mode activated.

Gene ontology analysis

Functional annotation clustering was conducted using official gene symbols in DAVID bioinformatics v6.8 (Huang et al. 2009). We used the Homo Sapiens model as background due to its more comprehensive pathway annotation. The analysis was carried out using the default categories (OMIM_DISEASE, COG_ONTOLOGY, UP_KEYWORDS, UP_SEQ_FEATURE, GOTERM_BP_DIRECT, GOTERM_CC_DIRECT, GOTERM_MF_DIRECT, BBID, BIOCARTA, KEGG_PATHWAY, INTERPRO, PIR_SUPERFAMILY, SMART) and medium stringency.

DATA ACCESS

The raw sequencing data generated in this study have been submitted to the NCBI BioProject database (https://www.ncbi.nlm.nih.gov/bioproject/) under accession number PRJNA630504.

AKNOWLEDGEMENTS

Funding for this project was provided by USDA-NIFA-AFRI grant no. 2017-67015-26297 to PJR. ChIP-seq data was generated as part of USDA-NIFA-AFRI grant no. 2015-43567015-22940 to HZ and PJR. MMH was supported by a USDA-NIFA National Needs Fellowship Grant (USDA-NIFA Competitive Grant Project no. 2014-38420-21796) and an Austin Eugene Lyons Fellowship.

DISCLOSURE DECLARATION

Authors declare no conflicts of interest.

REFERENCES

Abugessaisa I, Noguchi S, Hasegawa A, Kondo A, Kawaji H, Carninci P, Kasukawa T. 2019. refTSS: A Reference Data Set for Human and Mouse Transcription Start Sites. *Journal of Molecular Biology* **431**: 2407–2422.

Adiconis X, Haber AL, Simmons SK, Levy Moonshine A, Ji Z, Busby MA, Shi X, Jacques J, Lancaster MA, Pan JQ, et al. 2018. Comprehensive comparative analysis of 5′-end RNA-sequencing methods. *Nature Methods* **15**: 505–511.

Alles J, Fehlmann T, Fischer U, Backes C, Galata V, Minet M, Hart M, Abu-Halima M, Grässer FA, Lenhof H-P, et al. 2019. An estimate of the total number of true human miRNAs. *Nucleic Acids Res* **47**: 3353–3364.

Andersson L, Archibald AL, Bottema CD, Brauning R, Burgess SC, Burt DW, Casas E, Cheng HH, Clarke L, Couldrey C, et al. 2015. Coordinated international action to accelerate genome-to-phenome with FAANG, the Functional Annotation of Animal Genomes project. *Genome Biology* **16**: 57.

Batut P, Dobin A, Plessy C, Carninci P, Gingeras TR. 2013. High-fidelity promoter profiling reveals widespread alternative promoter usage and transposon-driven developmental gene expression. *Genome Res* **23**: 169–180.

Batut P, Gingeras TR. 2013. Rampage: Promoter Activity Profiling by Paired-end Sequencing of 5′-complete cDNAs. *Curr Protoc Mol Biol* **104**: Unit-25B.11.

Bevacqua RJ, Fernandez-Martín R, Savy V, Canel NG, Gismondi MI, Kues WA, Carlson DF, Fahrenkrug SC, Niemann H, Taboga OA, et al. 2016. Efficient edition of the bovine PRNP prion gene in somatic cells and IVF embryos using the CRISPR/Cas9 system. *Theriogenology* **86**: 1886-1896.e1.

Britt JH, Cushman RA, Dechow CD, Dobson H, Humblot P, Hutjens MF, Jones GA, Ruegg PS, Sheldon IM, Stevenson JS. 2018. Invited review: Learning from the future-A vision for dairy farms and cows in 2067. *J Dairy Sci* **101**: 3722–3741.

Carninci P, Sandelin A, Lenhard B, Katayama S, Shimokawa K, Ponjavic J, Semple CAM, Taylor MS, Engström PG, Frith MC, et al. 2006. Genome-wide analysis of mammalian promoter architecture and evolution. *Nat Genet* **38**: 626–635.

Consortium TBGS and A, Elsik CG, Tellam RL, Worley KC. 2009. The Genome Sequence of Taurine Cattle: A Window to Ruminant Biology and Evolution. *Science* **324**: 522–528.

Djureinovic D, Fagerberg L, Hallström B, Danielsson A, Lindskog C, Uhlén M, Pontén F. 2014. The human testis-specific proteome defined by transcriptomics and antibody-based profiling. *Mol Hum Reprod* **20**: 476–488.

Dobin A, Davis CA, Schlesinger F, Drenkow J, Zaleski C, Jha S, Batut P, Chaisson M, Gingeras TR. 2013. STAR: ultrafast universal RNA-seq aligner. *Bioinformatics* **29**: 15–21.

Engström PG, Suzuki H, Ninomiya N, Akalin A, Sessa L, Lavorgna G, Brozzi A, Luzi L, Tan SL, Yang L, et al. 2006. Complex Loci in Human and Mouse Genomes. *PLoS Genet* **2**: e47.

Ernst J, Kellis M. 2017. Chromatin state discovery and genome annotation with ChromHMM. *Nat Protoc* **12**: 2478–2492.

FANTOM Consortium and the RIKEN PMI and CLST (DGT), Forrest ARR, Kawaji H, Rehli M, Kenneth Baillie J, de Hoon MJL, Haberle V, Lassmann T, Kulakovskiy IV, Lizio M et al. 2014. A promoter-level mammalian expression atlas. *Nature* **507**: 462–470.

Gossett LA, Kelvin DJ, Sternberg EA, Olson EN. 1989. A new myocyte-specific enhancer-binding factor that recognizes a conserved element associated with multiple muscle-specific genes. *Mol Cell Biol* **9**: 5022–5033.

Guo J, Zhu P, Wu C, Yu L, Zhao S, Gu X. 2003. In silico analysis indicates a similar gene expression pattern between human brain and testis. *Cytogenet Genome Res* **103**: 58–62.

Guo JH, Huang Q, Studholme DJ, Wu CQ, Zhao Z. 2005. Transcriptomic analyses support the similarity of gene expression between brain and testis in human as well as mouse. *CGR* **111**: 107–109.

Heintzman ND, Stuart RK, Hon G, Fu Y, Ching CW, Hawkins RD, Barrera LO, Van Calcar S, Qu C, Ching KA, et al. 2007. Distinct and predictive chromatin signatures of transcriptional promoters and enhancers in the human genome. *Nat Genet* **39**: 311–318.

Heinz S, Benner C, Spann N, Bertolino E, Lin YC, Laslo P, Cheng JX, Murre C, Singh H, Glass CK. 2010. Simple combinations of lineage-determining transcription factors prime cis-regulatory elements required for macrophage and B cell identities. *Mol Cell* **38**: 576–589.

Huang DW, Sherman BT, Lempicki RA. 2009. Systematic and integrative analysis of large gene lists using DAVID bioinformatics resources. *Nat Protoc* **4**: 44–57.

Ju Z, Jiang Q, Wang J, Wang X, Yang C, Sun Y, Zhang Y, Wang C, Gao Y, Wei X, et al. 2020. Genome-wide methylation and transcriptome of blood neutrophils reveal the roles of DNA methylation in affecting transcription of protein-coding genes and miRNAs in E. coli-infected mastitis cows. *BMC Genomics* **21**: 102.

Kern C, Wang Y, Chitwood J, Korf I, Delany M, Cheng H, Medrano JF, Van Eenennaam AL, Ernst C, Ross P, et al. 2018. Genome-wide identification of tissue-specific long non-coding RNA in three farm animal species. *BMC Genomics* **19**: 684.

Kodzius R, Kojima M, Nishiyori H, Nakamura M, Fukuda S, Tagami M, Sasaki D, Imamura K, Kai C, Harbers M, et al. 2006. CAGE: cap analysis of gene expression. *Nat Methods* **3**: 211–222.

Langfelder P, Horvath S. 2008. WGCNA: an R package for weighted correlation network analysis. *BMC Bioinformatics* **9**: 559.

Lawrence M, Huber W, Pagès H, Aboyoun P, Carlson M, Gentleman R, Morgan MT, Carey VJ. 2013. Software for computing and annotating genomic ranges. *PLoS Comput Biol* **9**: e1003118.

Lepoivre C, Belhocine M, Bergon A, Griffon A, Yammine M, Vanhille L, Zacarias-Cabeza J, Garibal M-A, Koch F, Maqbool M, et al. 2013. Divergent transcription is associated with promoters of transcriptional regulators. *BMC Genomics* **14**: 914.

Li H, Durbin R. 2009. Fast and accurate short read alignment with Burrows-Wheeler transform. *Bioinformatics* **25**: 1754–1760.

Li H, Handsaker B, Wysoker A, Fennell T, Ruan J, Homer N, Marth G, Abecasis G, Durbin R, 1000 Genome Project Data Processing Subgroup. 2009. The Sequence Alignment/Map format and SAMtools. *Bioinformatics* **25**: 2078–2079.

Liao Y, Smyth GK, Shi W. 2014. featureCounts: an efficient general purpose program for assigning sequence reads to genomic features. *Bioinformatics* **30**: 923–930.

Love MI, Huber W, Anders S. 2014. Moderated estimation of fold change and dispersion for RNA-seq data with DESeq2. *Genome Biol* **15**: 550.

Meers MP, Adelman K, Duronio RJ, Strahl BD, McKay DJ, Matera AG. 2018. Transcription start site profiling uncovers divergent transcription and enhancer-associated RNAs in Drosophila melanogaster. *BMC Genomics* **19**: 157.

Null D, VanRaden PM, Rosen B, O'Connell J, Bickhart D. 2019. Using the ARS-UCD1.2 reference genome in U.S. evaluations. *Interbull Bulletin* 30–34.

Pertea M, Pertea GM, Antonescu CM, Chang T-C, Mendell JT, Salzberg SL. 2015. StringTie enables improved reconstruction of a transcriptome from RNA-seq reads. *Nat Biotechnol* **33**: 290–295.

Ramírez F, Ryan DP, Grüning B, Bhardwaj V, Kilpert F, Richter AS, Heyne S, Dündar F, Manke T. 2016. deepTools2: a next generation web server for deep-sequencing data analysis. *Nucleic Acids Res* **44**: W160–W165.

Rosen BD, Bickhart DM, Schnabel RD, Koren S, Elsik CG, Tseng E, Rowan TN, Low WY, Zimin A, Couldrey C, et al. 2020. De novo assembly of the cattle reference genome with single-molecule sequencing. *Gigascience* **9**.

Salimullah M, Sakai M, Mizuho S, Plessy C, Carninci P. 2011. NanoCAGE: a high-resolution technique to discover and interrogate cell transcriptomes. *Cold Spring Harb Protoc* **2011**: pdb.prot5559.

Tav C, Tempel S, Poligny L, Tahi F. 2016. miRNAFold: a web server for fast miRNA precursor prediction in genomes. *Nucleic Acids Res* **44**: W181-184.

Tong C, Chen Q, Zhao L, Ma J, Ibeagha-Awemu EM, Zhao X. 2017. Identification and characterization of long intergenic noncoding RNAs in bovine mammary glands. *BMC Genomics* **18**: 468.

Van Eenennaam AL, Weigel KA, Young AE, Cleveland MA, Dekkers JCM. 2014. Applied animal genomics: results from the field. *Annu Rev Anim Biosci* **2**: 105–139.

Wade JT, Grainger DC. 2014. Pervasive transcription: illuminating the dark matter of bacterial transcriptomes. *Nat Rev Microbiol* **12**: 647–653.

Weikard R, Hadlich F, Kuehn C. 2013. Identification of novel transcripts and noncoding RNAs in bovine skin by deep next generation sequencing. *BMC Genomics* **14**: 789.

Wucher V, Legeai F, Hédan B, Rizk G, Lagoutte L, Leeb T, Jagannathan V, Cadieu E, David A, Lohi H, et al. 2017. FEELnc: a tool for long non-coding RNA annotation and its application to the dog transcriptome. *Nucleic Acids Res* **45**: e57.

Yamashita R, Sathira NP, Kanai A, Tanimoto K, Arauchi T, Tanaka Y, Hashimoto S-I, Sugano S, Nakai K, Suzuki Y. 2011. Genome-wide characterization of transcriptional start sites in humans by integrative transcriptome analysis. *Genome Res* **21**: 775–789.